NASA TECHNICAL NOTE

NASA TN D-6123

NASA TN D-6123

COMPOSITION DISTRIBUTION AND EQUIVALENT BODY SHAPE FOR A REACTING, COAXIAL, SUPERSONIC HYDROGEN-AIR FLOW

by Griffin Y. Anderson, Anthony M. Agnone, and Wm. Roger Russin

Langley Research Center
Hampton, Va. 23365

NATIONAL AERONAUTICS AND SPACE ADMINISTRATION • WASHINGTON, D. C. • JANUARY 1971

1. Report No.	2. Government Accession No.	3. Recipient's Catalog No.
NASA TN D-6123		

4. Title and Subtitle	5. Report Date
COMPOSITION DISTRIBUTION AND EQUIVALENT BODY SHAPE FOR A REACTING, COAXIAL, SUPERSONIC HYDROGEN-AIR FLOW	January 1971
	6. Performing Organization Code
7. Author(s)	8. Performing Organization Report No.
Griffin Y. Anderson, Anthony M. Agnone (New York University), and Wm. Roger Russin	L-7498
9. Performing Organization Name and Address	10. Work Unit No.
NASA Langley Research Center Hampton, Va. 23365	722-03-10-01
	11. Contract or Grant No.
12. Sponsoring Agency Name and Address	13. Type of Report and Period Covered
National Aeronautics and Space Administration Washington, D.C. 20546	Technical Note
	14. Sponsoring Agency Code

15. Supplementary Notes

16. Abstract

Results of an experiment with an ambient-temperature Mach 2 hydrogen jet mixing and reacting with an ambient-temperature Mach 2 air stream are presented and analyzed. Combustion of the hydrogen jet was piloted by reaction in a low-velocity annular oxygen flow between the hydrogen and air flows. Pitot pressures measured in the air flow outside the mixing-reacting region were used with an inverse application of the method of characteristics to calculate streamlines and deduce an equivalent nonreacting-flow body shape to represent the burning jet. Expansion waves generated by a rectangular duct placed around the jet were found to produce no large change in the mixing and reaction between the hydrogen and air streams. Gas samples abstracted from the mixing-reacting region were used to match theoretical turbulent-mixing calculations with the experimental data. Streamlines from the inverse application of the method of characteristics and from mixing computations are identical outside the mixing region near the jet exit. Measured Mach number profiles across the flow for the nonburning and burning cases match mixing computations for the same value of turbulent viscosity, implying that chemical reaction does not affect mixing rate under the conditions of this experiment.

17. Key Words (Suggested by Author(s))	18. Distribution Statement
Turbulent mixing Hydrogen combustion Equivalent body Gas sampling	Unclassified – Unlimited

19. Security Classif. (of this report)	20. Security Classif. (of this page)	21. No. of Pages	22. Price*
Unclassified	Unclassified	41	$3.00

*For sale by the National Technical Information Service, Springfield, Virginia 22151

COMPOSITION DISTRIBUTION AND EQUIVALENT BODY SHAPE FOR A REACTING, COAXIAL, SUPERSONIC HYDROGEN-AIR FLOW

By Griffin Y. Anderson, Anthony M. Agnone,*
and Wm. Roger Russin
Langley Research Center

SUMMARY

Results of an experiment with an ambient-temperature Mach 2 hydrogen jet mixing and reacting with an ambient-temperature Mach 2 air stream are presented and analyzed. Combustion of the hydrogen jet was piloted by reaction in a low-velocity annular oxygen flow between the hydrogen and air flows. Pitot pressures measured in the air flow outside the mixing-reacting region were used with an inverse application of the method of characteristics to calculate streamlines and deduce an equivalent nonreacting-flow body shape to represent the burning jet. Expansion waves generated by a rectangular duct placed around the jet were found to produce no large change in the mixing and reaction between the hydrogen and air streams. Gas samples abstracted from the mixing-reacting region were used to match theoretical turbulent-mixing calculations with the experimental data. Streamlines from the inverse application of the method of characteristics and from mixing computations are identical outside the mixing region near the jet exit. Measured Mach number profiles across the flow for the nonburning and burning cases match mixing computations for the same value of turbulent viscosity, implying that chemical reaction does not affect mixing rate under the conditions of this experiment.

INTRODUCTION

The potential of supersonic-combustion ramjet propulsion for hypersonic flight has been recognized for more than a decade. (See refs. 1, 2, and 3.) Progress toward the realization of this potential for a specific application requires the development of practical compromises between many conflicting requirements, as discussed in reference 4. On the one hand, the desire for high engine performance over a range of flight speeds suggests the need for variable geometry with movable inlet ramps, combustor walls, and nozzle surfaces. On the other hand, the need for low engine weight, mechanical simplicity, and minimum cooling requirements dictates that variable geometry be held to a minimum.

---

*New York University.

Combustion-generated compression has been suggested in reference 5 as a means of varying inlet compression without variable geometry. Conceptually, the desired variations in the location and strength of specific portions of the inlet compression process are controlled by tailoring the distribution of fuel injection instead of changing the wall geometry. Even for a crude beginning, the design of an inlet employing combustion-generated compression requires the ability to predict the flow field surrounding a single fuel injector. A theoretical analysis which can be applied to this problem is available (ref. 6), but the results depend on the proper choice of constants to represent the turbulent mixing between the injected fuel and surrounding air. Further, the analysis is limited to situations in which no large radial pressure gradients exist and requires the axial static-pressure distribution as an input.

Once designed, an inlet employing combustion-generated compression poses additional problems in testing. In order to demonstrate performance, either the test hardware and facility must be suitable for producing combustion or some means of simulating the effects of combustion must be provided. One possible simulation technique is the use of an "equivalent body" to replace the fuel injector and the mixing and reacting region. Reference 7 presents an evaluation of this technique as applied to turbojet exhaust plumes of supersonic airplanes. In effect, the streamline displacement in the nonreacting flow surrounding the injector and combustion region is reproduced by supplying the proper streamline shape with a contoured wall. Simulation of the effects of combustion with an equivalent body is essentially the inverse application of the concept of combustion-generated compression to hypersonic-inlet design. Design of the inlet requires prediction of the flow field generated by mixing and combustion; testing of the inlet in aerodynamic facilities where combustion is not possible requires prediction of the equivalent body shape which simulates mixing and combustion.

An experiment was undertaken to explore combustion-generated compression with the ultimate goal of developing techniques for practical application to inlet and combustor design. To simplify the experimental setup and instrumentation, a simple axisymmetric geometry and ambient-temperature gas supplies were chosen. Specifically, the purpose of the experiment was threefold:

(1) To provide detailed measurements of aerodynamic effects outside the burning region caused by a mixing and reacting fuel jet and calculate its equivalent body shape

(2) To examine in at least a qualitative way the effect of externally generated waves on the mixing-reacting region

(3) To obtain pitot pressures and gas samples from the mixing-reacting region

Once the streamline shape for a mixing-reacting fuel jet is determined experimentally, a comparison with predictions of a mixing analysis such as the one presented in reference 6 can be made.

SYMBOLS

B	ratio of oxygen to nitrogen atoms relative to that in air
C	species mass fraction after complete reaction
F	fraction of hydrogen reacted
M	Mach number
$\mathcal{M}$	molecular weight
p	static pressure
p_t	total pressure
q	dynamic pressure
R	universal gas constant
r	radial coordinate measured from nozzle center line
r_j	centerbody or jet radius (1.09 cm)
T	static temperature
T_t	total temperature
V	velocity
x	axial coordinate measured from nozzle exit plane
α	species mass fraction
γ	ratio of specific heats
$\Delta\Theta$	angle between local flow direction and center line
ν	species volume fraction

ρ density

ψ Von Mises or streamline coordinate

Subscripts:

0 nozzle plenum

2 behind normal shock

∞ free stream

$\mathfrak{t}$ center line

e nozzle exit

H_2 hydrogen

H_2O water

N_2 nitrogen

O_2 oxygen

APPARATUS AND PROCEDURE

The experimental apparatus is shown schematically in figure 1. Dry air at ambient temperature is supplied from storage bottles to an axisymmetric, contoured, Mach 2 nozzle which has a cylindrical centerbody. The centerbody is supported by streamlined struts mounted within the nozzle plenum. Care was taken in the design to make the centerbody and its supports sufficiently rigid to prevent centerbody vibration of significant amplitude during operation of the nozzle. Coordinates for the nozzle contour were taken from reference 8 and scaled to give a 15-cm exit diameter. The nozzle exhausts to ambient pressure as a free jet, and air-supply pressure is adjusted to match the nozzle exit pressure with ambient pressure.

As shown in the detail inset of figure 1, the centerbody consists of a straight-walled outer tube and an inner tube having a 5° half-angle internal expansion tip with area ratio of approximately 2.2. The constant-area annulus between the inner and outer tubes is supplied with ambient-temperature oxygen from storage bottles at 0.008 kg/sec. The inner tube is supplied with ambient-temperature hydrogen from gas-tube trailers at

0.065 kg/sec. If one-dimensional flow is assumed, with these flow rates the oxygen velocity is subsonic at about 30 m/sec and the hydrogen velocity is supersonic (Mach number 2.3) at more than 2000 m/sec. The low-velocity oxygen and the blunt base of the outer tube form a region where combustion of the central hydrogen jet can stabilize once the flow is ignited.

Ignition of the flow is achieved by the following technique. Air flow to the nozzle and oxygen flow to the centerbody annulus are established. A small flow of fuel-rich hydrogen-air mixture (0.06 g/sec of hydrogen and 0.5 g/sec of air) is supplied to the inner tube. The mixture is ignited by a spark plug located at the entrance to the inner tube. The hot fuel-rich combustion products flow down the inner tube to its exit, where they mix and burn with the annular oxygen flow and surrounding air. With combustion established at the exit of the inner tube, hydrogen flow to the inner tube is increased to the desired value and air flow to the inner tube is stopped. Combustion between the hydrogen from the inner tube and the surrounding air flow continues, piloted by combustion in the low-velocity oxygen and base region of the outer tube.

Measurements in the cold flow field surrounding the mixing-reacting region of the flow were made with an uncooled pitot rake. The rake tubes had an outside diameter of 1.5 mm and a wall thickness of 0.25 mm. The measuring tip of each tube was flattened to an oval shape over a piece of 0.25-mm shim stock and the longer dimension of the oval was oriented perpendicular to the plane of the rake. The individual tubes were supported in a strut of wedge cross section with about 2.5-mm spacing between tube centers. The rake was mounted along a radial line in the flow and could be positioned at different axial locations by remote control. Pitot pressures were measured and gas samples collected in the mixing-reacting region of the flow with a single-tube water-cooled probe.

Externally generated waves intersecting the mixing-reacting core of the test flow were produced by adding the rectangular-cross-section duct shown in figure 2 to the apparatus. The side walls of the duct are parallel, but the top and bottom walls each diverge at an angle of 5° with respect to the center line. When mounted with its center line on the center line of the flow and its entrance plane in the plane of the centerbody tip, this "wave duct" produced expansions propagating from the leading edges of the top and bottom walls toward the center line of the flow. The ratio of the air flow entering the duct to the hydrogen flow in the jet is approximately stoichiometric. The wave duct was instrumented with static-pressure taps on the center line of each wall as indicated in figure 2.

The water-cooled probe and gas-sample collection system are shown schematically in figure 3. Coolant for the probe was supplied at 400° K and the line from the probe to the sample bottle was insulated and electrically heated to 400° K in an attempt to avoid condensing any water present in the gas withdrawn by the probe. Gas samples were

collected in unheated 150-cm^3 stainless-steel bottles by the following procedure. The bottle was evacuated and valves at each end were closed. The bypass around the sample bottle to the vacuum pump was opened, and the probe was placed in the desired position with coolant flowing and sample-line heaters on. Nozzle air flow and combustion were initiated. After approximately 30 seconds' delay to allow representative gas to reach the bottle, the bottle inlet valve was open and the bypass closed. The bottle pressure was allowed to rise to a steady value (usually within 10 to 20 seconds), the bottle inlet valve was closed, and the pitot pressure was recorded.

This procedure was varied in the collection of two samples in order to check the gas analysis technique. Instead of allowing sample gas to flow into a dead-end sample bottle, the valve between the sample bottle and vacuum pump was left open and sample gas was allowed to flow through the bottle. Since the bottle was not heated, condensation and collection of water from the sample gas might be expected. Once a sample bottle had been filled, it was removed from the system and replaced by another bottle. The sample-bottle contents were analyzed away from the site of the experiment in a mass spectrometer. Before withdrawing a sample from the bottle into the mass spectrometer, the bottle and inlet piping to the instrument were electrically heated to 400° K. For the contents of a given sample bottle the mass spectrometer analysis is accurate within ±1 percent.

In the experiment, data were collected in the following manner. With either the uncooled rake, the wave duct, or the cooled probe mounted in the desired location, nozzle air flow and combustion were established. After a few seconds' delay to allow pressure readings to stabilize, data recording was initiated. When recording was completed, the hydrogen flow was stopped and the rake or probe was set in a new position. Repeatability of the mass flow rates of hydrogen and oxygen from run to run was measured with orifice plates and found to be better than ±3 percent. The nozzle supply pressure was repeated within ±1 percent from run to run. Pitot pressures from the cooled probe and the uncooled rake and static pressures from the wave duct were measured with strain-gage pressure transducers. The absolute accuracy of these measurements is estimated to be ±2 percent. However, since the uncooled-rake pitot pressures were commutated by pressure scanning valves and measured with the same transducer, differences between these readings in the same run should be significant to the resolution of the recording device, or approximately ±0.1 percent.

RESULTS AND DISCUSSION

Uncooled-Rake Measurements

Schlieren photographs of the experimental flow field are shown in figure 4. In the nonburning case an expansion fan and recompression shock in the main air flow at the tip

of the nozzle centerbody are clearly visible. Also, oblique shocks from the lip of the inner tube are visible in the hydrogen jet, confirming that the jet is supersonic. In the burning case the expansion and recompression in the main air flow are not seen. Instead, a weak wave starts at the tip of the centerbody and propagates out into the main air flow. The waves in the hydrogen jet are still visible but are obscured to some extent by the large density gradient in the annular combustion region surrounding the hydrogen jet.

Pitot-pressure data taken with the uncooled rake for the nonburning and burning flows shown in figure 4 are given in table I. In order to calculate the equivalent body shape for these flows, the computer program described in reference 7 was used. The program requires as input the distribution of Mach number and flow direction along a line in the flow and constructs a characteristic net from the data line toward the center line. The construction assumes perfect-gas relations so that the flow generated is an equivalent (in that it has the same Mach number and flow direction along the data line) flow field of uniform composition and total temperature. The method used to calculate Mach number and flow direction from the rake measurements is presented in appendix A.

In both the nonburning and burning schlieren photographs of figure 4 some weak waves originating upstream of the nozzle exit plane are visible. Further evidence of nonuniformity in the air flow at the nozzle exit plane is shown in figure 5. There the local Mach number at the nozzle exit, calculated according to reference 9 from the ratio of rake pitot pressure to nozzle plenum pressure, is plotted as a function of radial location. In the portion of the flow outside $r/r_j = 3.9$ the local Mach number has a mean value near 1.97. Nearer the nozzle centerbody, the Mach number approaches 2.05. The importance of even small nonuniformities in the flow originating in the nozzle cannot be overemphasized. Since the data are to be used to determine the effect of the jet mixing and reaction on the surrounding air flow, any variations due to nonuniformity in nozzle flow and not related to the jet mixing and reaction must be eliminated from the data.

Typical pitot data along a line parallel to the center line are shown by the symbols in figure 6 for the nonburning and burning cases. If these data are used directly, large turning of streamlines away from the center line is calculated for both the nonburning and burning cases. Since the calculation assumes uniform flow approaching the data line, changes in pressure due to compressions and expansions originating in the nozzle are incorrectly taken as arising from waves generated near the axis of the flow. For instance, the weak compression in the nozzle flow noted in figure 4 raises pressure along the data line by turning the flow toward the center line. But the calculation incorrectly interprets this rise in pressure as due to a compression of the opposite family originating near the center line of the flow which turns the flow away from the center line.

In order to get even a qualitative picture of the equivalent streamline shape for the nonburning and burning cases, the data had to be corrected to remove the effect of the

strongest waves from the nozzle. By careful study of the schlieren photographs reproduced in figure 4 and all the uncooled-rake data, the approximate strength of the wave in figure 4 which originates in the nozzle was estimated. The change in pressure due to this wave was then subtracted from the measured pressure along the data line, and the local Mach number and flow direction were calculated as discussed in appendix A. The corrected data which were used to calculate values for input to the computer program described in reference 7 are shown by the lines in figure 6. The uncorrected and corrected pitot-pressure ratios and the calculated Mach number and flow direction are presented in table II.

Computed streamlines are plotted in figure 7. Note that the scale of the radial location is five times that of the axial location to accentuate streamline deflection. In the nonburning case the flow expands toward the center line, recompresses, and then gradually diverges from the center line, in agreement with the effects indicated in figure 4. With burning no expansion and recompression occur; the streamlines simply turn away from the center line. The location of the equivalent-body surface, ideally the streamline that starts on the center line in the uniform parallel flow assumed ahead of the nozzle exit plane, was estimated by extrapolation from streamlines starting near the center line since the equations used in the inverse application of the method of characteristics are indeterminate at the center line. For the burning case in figure 7 the streamline nearest the center line represents the estimated equivalent-body shape for the mixing-reacting jet. The equivalent body is essentially conical with a half-angle of about 6°.

Wave Duct

Externally generated waves intersecting the mixing-reacting region were produced by installing the wave duct in the nozzle exit plane as described in the section entitled "Apparatus and Procedure." Pressures measured on the walls of the wave duct divided by nozzle-exit static pressure are presented in figure 8 for the nonburning and burning jet. In the nonburning case the pressure generally decreases along the length of the duct. Peaks and valleys in pressure due to shocks and expansions traveling back and forth across the duct are evident at a spacing of 5 or 6 jet radii. In the burning case a general rise of pressure along the length of the duct is noted. Peaks and valleys in pressure indicating the presence of waves are still evident but at somewhat smaller axial spacing than in the nonburning case. Also, the range in pressure on the four walls of the duct at a given axial location is nearly twice as great in the burning case as in the nonburning case.

Detailed prediction of the pressure distributions in figure 8 would indeed be a formidable task. The flow is three dimensional, it is nonuniform in velocity and composition,

and the effects of chemical reaction are apparently important. However, at least a qualitative representation of the general trend and level of pressure in the wave duct should be obtainable with a one-dimensional analysis. With this goal in mind a one-dimensional analysis was written following the development in chapter 8 of reference 10. The analysis essentially consists of writing equations for the conservation of mass, momentum, and energy in an increment of length in a one-dimensional channel. Real-gas thermodynamic properties for hydrogen-air mixtures reacted to a specified degree are used in the analysis. A computer program was prepared to implement the analysis. Input to the program includes the cross-sectional area distribution and the combustion distribution with axial distance as well as the properties of the entering air and hydrogen streams.

The wave-duct static-pressure distribution computed for the nonburning case is shown in figure 9. The data points shown are the average of the pressures measured on the four walls of the duct at each axial location. The trend of the data is represented fairly well by the theoretical one-dimensional pressure distribution. The sharp initial rise of the theoretical curve results from completely mixing the entering hydrogen and air streams in the first step of the theoretical calculation. Instant mixing is required for a one-dimensional representation but, of course, does not occur in the experiment. Actual measurements would not be expected to show an initial pressure rise similar to that shown by the theory.

In order to compute the static-pressure distribution in the wave duct with burning, the axial distribution of chemical reaction must be specified. From the uncooled-rake data discussed in the preceding section, an equivalent body with a nearly conical surface was deduced for the burning case. If the cross-sectional area of the equivalent body is taken as proportional to the amount of fuel reacted and the presence of the wave duct does not greatly affect the mixing and combustion distribution, then the fraction of fuel reacted should be proportional to the square of the distance from the nozzle exit:

$$F \propto \left(\frac{x}{r_j}\right)^2 \tag{1}$$

The static-pressure distribution resulting from this assumption is shown in figure 10 for three different levels of fuel reacted at the end of the wave duct. The symbols represent the average of the measured pressures on the four walls of the wave duct at each axial location. The one-dimensional theoretical calculation gives a fair representation of the trend of the data but of course does not predict the pressure excursion due to waves. As indicated in the figure, the theoretical pressure distribution is quite sensitive to the total amount of fuel assumed to react. If the fraction of fuel reacted at the end of the duct exceeds 0.055, the one-dimensional theoretical computations indicate choking. Since no evidence of choking was observed in the experiment, the heat addition in the wave duct is likely to be less than that corresponding to $F = 0.055$.

Cooled-Probe Measurements

Since data acquisition with the single-tube cooled probe (particularly gas-sample collection) consumed considerable run time, only limited data were obtained. The data consist of radial surveys of pitot pressure for the nonburning and burning cases at two axial locations and a radial survey of composition in the burning case at one axial location. The pitot-pressure data are shown in figure 11. Uncooled-rake data for the same axial locations are included to extend the profiles into the outer portion of the flow. The profiles at the two axial locations have the same qualitative shape, but substantial differences are noted between the nonburning and burning data. The region of low pitot pressure for the burning case is lower, wider, and farther displaced from the center line of the flow than that for the nonburning case. The pitot-pressure data are discussed and analyzed further after treatment of the gas-sample data.

Gas-sample data.- Results of the mass-spectrometer analysis of the sample-bottle contents are presented in figure 12. The hydrogen concentration is a maximum near the center line and decreases sharply to zero in the region near 2 jet radii from the center line. Nitrogen and oxygen concentrations show the opposite trend, with constant values near those for air at large distance from the center line and values near zero at the center line. It is interesting to note that in the region near 2 jet radii from the center line, samples contain both unreacted hydrogen and oxygen. The water concentration is a maximum at about $1\frac{1}{2}$ jet radii from the center line and decreases to near zero at the center line and at large distances from the center line. Water concentrations for the two samples that were pumped through a cold sample bottle, shown by the flagged symbols, are substantially higher than the rest of the data, as expected. However, even these two points are significantly below 0.35, the water volume fraction expected for combustion of a stoichiometric hydrogen-air mixture.

To investigate the cause of the low water concentrations found in the sample bottles, the ratio of oxygen atoms to nitrogen atoms in each sample was calculated. Since each sample is a mixture of hydrogen from the center jet, air from the outer stream, and perhaps some oxygen injected from the oxygen annulus, the ratio of oxygen to nitrogen atoms should be at least equal to the ratio of oxygen to nitrogen atoms in air. This should be true regardless of chemical composition, provided only that macroscopic turbulent transport dominates over molecular diffusion. The calculated ratio of oxygen to nitrogen atoms divided by that ratio for air is presented in the upper portion of figure 13. Since some pure oxygen is being injected, the ratio plotted should be greater than or equal to 1 for all samples. However, values significantly less than 1 occur in the region near 2 jet radii from the nozzle center line, indicating a loss of oxygen atoms in the sample collection or analysis process. Although electric heating and insulation were used to prevent condensation of water from the sample gas flowing to the bottle, cold regions of tubing

may not have been eliminated. The loss of oxygen atoms is probably due to condensation of water in cold regions of the sample line. Higher concentrations of water measured in the two pumped samples demonstrate water removal from the sample gas by the cold sample bottle and also confirm the ability of the gas analysis technique to record water concentrations approaching the level expected.

In order to make further use of the gas-sample data presented in figure 12, a correction was made to the measured composition to account for oxygen depletion. The correction consisted of adding enough water to each measured composition to make the ratio of oxygen to nitrogen atoms at least equal to that of air. A detailed description of the treatment of the gas-sample data is included in appendix B. In the lower part of figure 13 the corrected water concentration is plotted along with the water concentration measured in the sample bottles. As can be seen, the correction produces a substantial change in both the magnitude and location of the peak in the water-concentration profile. The peak of the corrected water-concentration profile is higher and farther from the center line than the peak of the uncorrected data. In the rest of this report the corrected composition, with the ratio of oxygen to nitrogen atoms greater than or equal to that of air, will be taken as representative of the average gas composition ingested by the probe in the experiment.

It should be noted that the peak value of the corrected water concentration is still below 0.35, the maximum water concentration expected from combustion of a hydrogen-air mixture. This remaining difference is due to the unreacted hydrogen and oxygen found in the sample-bottle analysis. The degree to which a gas sample is reacted can be represented quantitatively by the ratio of the water present to the amount that would be present if the sample were completely reacted. This ratio, the "fraction reacted," was computed for the corrected gas composition and is shown in figure 14 as a function of radial location. The fraction reacted is substantially less than 1 at distances near 2 jet radii from the center line.

Incompletely reacted gas samples could result for a number of reasons. First, since combustion is occurring at a finite rate, reacting gas might enter the probe, be quenched by the cooled probe walls, and contribute unreacted hydrogen and oxygen to the sample-bottle contents. The probe, however, has a blunt tip and a simple cylindrical entrance, and the velocity of the sample gas entering the probe is less than one-twentieth of the local stream velocity. Therefore, it is likely that any partial reaction in the gas approaching the probe was completed in the process of entering the probe tip. A second possibility is that the unreacted hydrogen and oxygen found in the sample bottle entered the probe tip at different times. (See refs. 11 and 12.) In an inhomogeneous turbulent flow the probe could be expected to see at one instant a fuel-rich mixture and at another instant a fuel-lean mixture. Even though each of these mixtures might be completely

reacted and the time-average composition might be stoichiometric, unburned fuel and oxidizer would enter the probe. Once in the probe and cooled, the hydrogen and oxygen would mix without reacting on the way to the sample bottle and become part of the time-average composition ingested by the probe.

Mixing analysis.- The incompletely reacted gas composition that was measured poses some difficulty in relating the data to theoretical predictions. As can be seen in the schlieren photographs of figure 4 or the pitot-pressure profiles in figure 11, the physical location of the mixing-reacting region depends on how much reaction is occurring. Therefore, theoretical predictions of composition in terms of radius would have to include proper representation of the local fractions reacted, as plotted in figure 14. Finite-rate chemical computations, although they provide a means of computing locally incomplete reactions, are not expected to be relevant to the present data. The fraction reacted could be correlated with local equivalence ratio or some other parameter and used with equilibrium chemistry to represent the data. However, since a composition profile was measured at only one axial location, this procedure was not considered warranted. Instead, the measured composition can be compared in terms of the Von Mises or streamline coordinate (ref. 6), which depends on the distribution of the jet and surrounding fluid but not on the completeness of chemical reaction. The streamline coordinate ψ was calculated for the data by the procedure given in appendix B. For an axisymmetric flow, the value of ψ at a given point is proportional to the square root of the mass flow of fluid contained within that radius.

The composition of completely reacted gas in terms of mass fractions is shown plotted against streamline coordinate in figure 15. Theoretical composition profiles calculated by the computer program presented in reference 6 are shown in figure 15 along with the data. For the theoretical calculations the Prandtl and Lewis numbers were assumed to be 1, and the eddy viscosity model recommended in reference 13 was adopted. The model is

$$\epsilon_t = kb(\rho V)_{\ell} \tag{2}$$

A value of 0.005 was used for the constant factor k. The parameter b is a mixing-zone width defined by particular values of velocity in the velocity profile as described in reference 13. The theory was fitted to the data by matching the location and width of the peak in the water distribution. As indicated in the figure the composition data were all shifted 0.038 $(kg/sec)^{1/2}$ toward the center line in order to match the theoretical distribution. This increment in ψ corresponds to a physical distance of 0.24 cm and is well within the precision with which the center line of the flow could be estimated in alining the transverse mechanism of the probe at this axial location (27 cm from the nozzle exit).

As can be seen in figure 15, the data and theoretical composition profile are in fair agreement. Near the center line the data show higher water concentration and lower

hydrogen concentration than the theory. However, in the theoretical calculations no satisfactory way could be found to represent the proper mass flow of oxygen injected from the oxygen annulus. Calculations were made simply for hydrogen mixing in air, and some difference between the data and theory should be expected in the center portion of the flow where the total amount of oxygen present is of the same order as the injected oxygen.

The local Mach number in the burning region is compared with the theoretical Mach number in figure 16. The local Mach number was calculated from the pitot-pressure data by means of the tables in reference 9, assuming a static pressure of 1 atmosphere and a ratio of specific heats equal to 1.4. Data and theory agree fairly well, with the data generally falling slightly above the theory. This difference is expected because the theoretical calculation assumes chemical equilibrium, whereas the data are representative of a flow which is incompletely reacted on the average. The additional heat release in a constant-pressure process would be expected to reduce the local Mach number slightly.

As a test of the corrected composition profiles and the assumptions used in computing the streamline coordinate, the total hydrogen flow and reacted hydrogen flow represented by the data were computed. For this calculation the center line of the data was shifted as shown in figure 15. The total hydrogen flow, including both unreacted hydrogen and hydrogen present in water, is 6 percent less than the flow to the hydrogen jet measured by the orifice plate. The hydrogen present in water amounts to 0.055 of the total hydrogen flow. This fraction is of the same order as the fraction reacted in the one-dimensional calculations for the wave duct and implies that the wave duct has little effect on the amount of mixing and reaction taking place.

Further comparison with mixing theory can be made for the nonburning pitot data as shown in figure 17, where Mach number, calculated from measured pitot pressure as in the burning case, is plotted against radial location. Chemical reaction was eliminated from the theoretical calculations by substituting nitrogen for air. All other input to the calculation was kept the same as for the burning case except the constant in the eddy viscosity model, which was increased by 20 percent to make the actual viscosity the same as for the burning case. In the burning case, heat release causes streamline divergence, which does not occur in the nonburning case. Thus, the value of the mixing zone width b in equation (2) is smaller in the nonburning case than in the burning case; and to keep the same value of eddy viscosity, the factor k must be increased proportionally.

Agreement between data and theory is fair. At 12 jet radii from the nozzle exit the data near the center line fall above the theory, while at 25 jet radii the data near the center line fall below the theory. These differences are a result of the expansion and recompression observed in the schlieren photograph of the nonburning case in figure 4. In the input to the theoretical calculations no attempt was made to simulate the changes

in static pressure associated with these waves. The cooled-probe data shown in figure 17 have been shifted toward the center line a distance corresponding to the ψ shift used with the data for the burning case in figures 15 and 16. The agreement between data and theory on the location of the minimum Mach number in figure 17 implies that there is no large difference in mixing between the nonburning and burning flow fields of this experiment.

Streamline comparison.- The streamlines for the nonburning flow field corresponding to the Mach number profiles presented in figure 17 are essentially straight lines diverging very slightly from the center line of the flow. The mixing computation did not include expansion toward the center line and recompression, since static pressure was assumed to be constant throughout the flow. However, the streamline deflection due to mixing alone is not as large as that shown downstream of the expansion and recompression region in the top part of figure 7. Apparently the quantity of data obtained with the uncooled rake and the quality of the nozzle flow field were not sufficient for precise streamline determination.

The streamlines calculated by the inverse application of the method of characteristics and the streamlines computed in the theoretical mixing calculation for the burning case are compared in figure 18. Streamlines calculated from the characteristic net are shown by solid lines, and streamlines from the mixing calculations are shown by the dashed lines. The outer edge of the mixing-reacting region predicted by the mixing theory is shown by the double dashed line. To the left of that line both theoretical calculations treat essentially the same fluid and can be compared directly; to the right of that line the two sets of streamlines should show differences due to mixing and reaction.

Outside the outer edge of the mixing-reacting region the streamlines are identical at axial distances of less than 8 jet radii. Farther downstream the streamlines from the inverse application of the method of characteristics show greater deflection than the streamlines from the mixing calculation, as was found for the nonburning case. Since equilibrium chemistry was assumed in calculating the mixing streamlines in figure 18, they should show slightly greater deflection due to heat release than the actual streamlines in the flow. Again it is apparent that the quantity of uncooled-probe data and the uniformity of the nozzle flow field were not sufficient for accurate streamline prediction by means of the inverse application of the method of characteristics, at least beyond 5 or 10 jet radii from the nozzle exit plane.

Inside the outer edge of the mixing-reacting region substantial differences between the two sets of streamlines are noted, as expected. The equivalent-flow streamlines continue turning away from the center line and move closer together with increasing distance downstream. The mixing streamlines, on the other hand, turn back toward the center line and spread apart in a short zone parallel to the outer edge of the mixing

region. This turning toward the center line and divergence is a result of the heat addition computed for the mixed part of the flow in the mixing calculation.

CONCLUDING REMARKS

Experimental measurements from the flow field produced by a Mach 2 ambient-temperature hydrogen jet mixing and reacting with a Mach 2 ambient-temperature air stream have been presented and analyzed. Data obtained with the uncooled pitot rake were found to be inadequate for direct use in calculating equivalent nonreacting-flow streamlines, largely because of nonuniformities in the nozzle flow field. The rake data were corrected with the aid of schlieren photographs, allowing the equivalent nonreacting-flow streamlines to be determined approximately. From these calculations the mixing and reacting jet was found to be equivalent to a conical body with a half-angle of 6°.

A duct with diverging walls was placed around the jet to produce waves intersecting the mixing-reacting region. The static-pressure distribution in the duct could be predicted reasonably well with a simple one-dimensional analysis. In the burning case, the amount of fuel burned was taken as proportional to the square of the distance from the jet exit, as suggested by the equivalent body shape. Burning more than 5.5 percent of the hydrogen entering the duct caused choking in the one-dimensional calculation. This quantity of fuel is of the same order as the reacted fuel found by integrating the profile data obtained with the cooled probe without the wave duct mounted. The agreement implies that the presence of the wave duct has little effect on the mixing and reaction occurring in the flow field of this experiment.

Gas samples abstracted with a cooled probe from the mixing-reacting region of the flow were found to be deficient in oxygen atoms. The oxygen depletion was attributed to loss of water from the samples by condensation, in spite of precautions taken in sample collection and analysis to prevent condensation. Samples were also found to contain unreacted hydrogen and oxygen. When corrected for water loss and completely reacted, the composition data could be matched to theoretical profiles computed with turbulent mixing theory by choosing the proper eddy viscosity. In further support of the corrections to the data, the integrated total hydrogen flow in the profile measured by the cooled probe was found to be 6 percent less than the metered flow supplied to the jet. Mach number profiles for the nonburning and burning cases matched theoretical computations for the same value of eddy viscosity. This result implies that there is no large difference in mixing between the nonburning and burning flow fields of this experiment.

Langley Research Center,
National Aeronautics and Space Administration,
Hampton, Va., November 30, 1970.

APPENDIX A

UNCOOLED-RAKE DATA AND ANALYSIS

In order to construct a uniform-composition, nonreacting flow field equivalent to the experimental flow by using the analysis of reference 7, the distribution of Mach number and flow direction along a line in the flow field is required. For convenience a data line parallel to the center line of the flow was chosen. Two operations on the uncooled-rake data were required to arrive at input for the calculation. First, the influence of waves originating in the nozzle on the pitot pressure along the data line was estimated and removed from the data. Second, on the basis of assumptions about the nature of the flow along the data line, the distributions of Mach number and flow direction were calculated from the pitot pressure and nozzle plenum pressure.

Waves originating in the nozzle were treated in the following manner. A grid of pitot-measurement locations was drawn to scale and laid over a schlieren photograph of the flow. Waves approaching the data line were followed back to a region where they crossed a radial survey, and wave strength was estimated from the difference between readings of adjacent tubes on opposite sides of the wave. The success of this technique depends on finding a region of radial survey where the local pressure variation results primarily from the nozzle wave. In the region near the data line, waves originating from both the mixing-reacting region and the nozzle flow are found. By tracing the nozzle waves away from the center line, their approximate strength can be determined and then removed from the data in the region of interest. The pitot pressure along the data line and the corrected pitot data are presented in table II for the nonburning and the burning case. Note that since the nonburning and burning flow fields are different, the location of the correction on the data line is different for the two flows.

The Mach number and flow direction along the data line were calculated from the pitot pressure by the following procedure. Since the data line chosen is more than 3 jet radii from the center line, the flow can be treated locally as two-dimensional for a good approximation in the region near the jet exit. If it is further assumed that waves are weak, so that the flow is essentially isentropic, linearized relations for small perturbations in two-dimensional supersonic flow (such as those derived in chapter 14 of reference 10) can be used.

From equation (14.12b) of reference 10,

$$\frac{p - p_\infty}{\frac{1}{2}\rho_\infty V_\infty^2} = \frac{2(\Delta\Theta)}{\sqrt{M_\infty^2 - 1}} \tag{A1}$$

where $\Delta\Theta$ is in radians. Substituting q_∞ for $\frac{1}{2}\rho_\infty V_\infty^2$ and solving for $\Delta\Theta$ in degrees yields:

$$\Delta\Theta = \frac{90}{\pi}\sqrt{M_\infty^2 - 1}\,\frac{\left(p/p_{t,\infty}\right) - \left(p_\infty/p_{t,\infty}\right)}{q_\infty/p_{t,\infty}} \tag{A2}$$

The values of M_∞, $p_\infty/p_{t,\infty}$, and $q_\infty/p_{t,\infty}$ were interpolated from the tables in reference 9 for the ratio of pitot to nozzle pressure on the data line in the nozzle exit plane. The Mach number and value of $p/p_{t,\infty}$ at each value of x/r_j were determined from the tables in reference 9 for the local corrected ratio of pitot pressure to nozzle plenum pressure. In order to provide a sufficiently fine grid for the inverse method of characteristics calculation, the pitot pressures were interpolated linearly in the axial direction. The distributions of local Mach number and flow direction computed by this procedure are included in table II.

APPENDIX B

GAS-SAMPLE DATA ANALYSIS

The mass-spectrometer analysis of the sample-bottle contents provided the composition of each gas sample in terms of volume fractions of hydrogen, water vapor, nitrogen, and oxygen. The ratio of oxygen to nitrogen atoms for the sample-bottle contents divided by that ratio for air is

$$B = \frac{\left(2\nu_{O_2} + \nu_{H_2O}\right)\Big/0.2095}{\left(2\nu_{N_2}\right)\Big/0.7808} \tag{B1}$$

where the volume fractions of oxygen in air (0.2095) and nitrogen in air (0.7808) are taken from reference 14. In correcting the sample-bottle composition to account for oxygen depletion through water loss, the number of moles of water that should have been measured was calculated from equation (B1) by assuming $B = 1$:

$$n_{H_2O} = 2\left(\frac{0.2095}{0.7808}\,\nu_{N_2} - \nu_{O_2}\right) \tag{B2}$$

Corrected volume fractions for the sample were then calculated by renormalizing the sample-bottle hydrogen, nitrogen, and oxygen volume fractions and the computed number of moles of water vapor. These calculations were made only for the sample-bottle compositions with values of B less than 1 and for the pumped samples.

The molecular weight of the sample is

$$\mathcal{M} = \sum_i \nu_i \mathcal{M}_i \tag{B3}$$

and sample mass fractions were calculated from sample volume fractions by the formula

$$\alpha_i = \nu_i \frac{\mathcal{M}_i}{\mathcal{M}} \tag{B4}$$

The degree to which the samples were completely reacted was determined as follows. The ratio of the mass of unreacted oxygen to the mass of unreacted hydrogen in each sample was calculated. For fuel-lean samples $\left(\alpha_{O_2}/\alpha_{H_2} > 8\right)$, after complete reaction the species mass fractions are

$$\left.\begin{aligned} C_{H_2} &= 0 \\ C_{H_2O} &= \alpha_{H_2O} + 9\alpha_{H_2} \\ C_{O_2} &= \alpha_{O_2} - 8\alpha_{H_2} \end{aligned}\right\} \tag{B5}$$

For fuel-rich samples $\left(\alpha_{O_2}/\alpha_{H_2} < 8\right)$, after complete reaction the species mass fractions are

$$\left.\begin{aligned} C_{H_2} &= \alpha_{H_2} - \frac{1}{8}\alpha_{O_2} \\ C_{H_2O} &= \alpha_{H_2O} + \frac{9}{8}\alpha_{O_2} \\ C_{O_2} &= 0 \end{aligned}\right\} \tag{B6}$$

Since nitrogen does not enter into any reactions considered, the nitrogen mass fraction after complete reaction is equal to the corrected nitrogen mass fraction for both fuel-lean and fuel-rich samples:

$$C_{N_2} = \alpha_{N_2} \tag{B7}$$

The degree of reaction is then simply

$$F = \frac{\alpha_{H_2O}}{C_{H_2O}} \tag{B8}$$

The Von Mises or streamline coordinate was calculated for the gas-sample data by the following procedure. First an estimate of the local total temperature in the reacting flow was made on the basis of the composition and degree of reaction. For the corrected composition the temperature rise for combustion to equilibrium ΔT_c of each sample was determined from reference 15. The local total temperature was taken as

$$T_t = 300 + F\left(\Delta T_c\right) \tag{B9}$$

Next the Mach number was estimated from the tables in reference 9 by using the measured pitot pressure and assuming a static pressure of 1 atmosphere and a ratio of specific heats equal to 1.4. The local velocity and density were then calculated with the aid of the tables in reference 9 and the following relations:

$$V = M\sqrt{\gamma \frac{R}{\mathcal{M}} T_t \frac{T}{T_t}} \tag{B10}$$

$$\rho = \frac{p\mathcal{M}}{RT_t \frac{T}{T_t}} \tag{B11}$$

The Von Mises or streamline coordinate is defined in reference 6 for an axisymmetric flow as

$$\psi \equiv \sqrt{2 \int_0^r \rho V r \, dr} \tag{B12}$$

For the gas-sample data the integral was approximated numerically as shown in the following sketch:

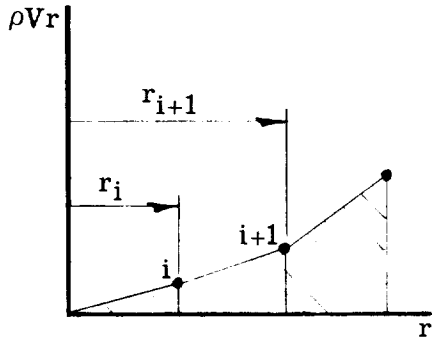

Then ψ was calculated from

$$\psi_n = \sqrt{2 \sum_{i=1}^{n} \left[\frac{(\rho V r)_{i+1} + (\rho V r)_i}{2} \left(r_{i+1} - r_i \right) \right]} \tag{B13}$$

If more than one gas sample, and hence more than one value of $\rho V r$ was available at a given radius, an average value of $\rho V r$ was used in calculating ψ.

REFERENCES

1. Weber, Richard J.; and MacKay, John S.: An Analysis of Ramjet Engines Using Supersonic Combustion. NACA TN 4386, 1958.

2. Mager, A.; and Baker, J.: On Efficient Utilization of Supersonic Combustion in Ramjets. Vol. II of Proceedings of Second Symposium on Advanced Propulsion Concepts, AFRD-60-2519, U.S. Air Force, Oct. 1959, pp. 29-48.

3. Ferri, Antonio: Possible Directions of Future Research in Air-Breathing Engines. Combustion and Propulsion Fourth AGARD Colloquium, A. L. Jaumotte, A. H. Lefebvre, and A. M. Rothrock, eds., Pergamon Press, 1961, pp. 3-15.

4. Henry, J. R.; and McLellan, C. H.: The Air-Breathing Launch Vehicle for Earth-Orbit Shuttle – New Technology and Development Approach. Paper presented at AIAA Advanced Transportation Meeting, Cocoa Beach, Florida, Feb. 1970.

5. Ferri, Antonio; and Fox, Herbert: Analysis of Fluid Dynamics of Supersonic Combustion Process Controlled by Mixing. Twelfth Symposium (International) on Combustion, Combustion Inst., 1969, pp. 1105-1113.

6. Diffusion Controlled Combustion for Scramjet Application. Tech. Rep. 569 (Contract No. NAS1-5117), Gen. Appl. Sci. Lab., Inc., Dec. 1965.
   Edelman, R.: Part I – Analysis and Results of Calculations.
   Hopf, H.; and Fortune, O.: Part II – Programmer's Manual.

7. Putnam, Lawrence E.; and Capone, Francis J.: Experimental Determination of Equivalent Solid Bodies to Represent Jets Exhausting Into a Mach 2.20 External Stream. NASA TN D-5553, 1969.

8. Clippinger, R. F.: Supersonic Axially Symmetric Nozzles. Rep. No. 794, Ballistic Res. Lab., Aberdeen Proving Ground, Dec. 1951.

9. Ames Research Staff: Equations, Tables, and Charts for Compressible Flow. NACA Rep. 1135, 1953. (Supersedes NACA TN 1428.)

10. Shapiro, Ascher H.: The Dynamics and Thermodynamics of Compressible Fluid Flow. Vol. I. Ronald Press Co., c.1953.

11. Hawthorne, W. R.; Weddell, D. S.; and Hottel, H. C.: Mixing and Combustion in Turbulent Gas Jets. Third Symposium on Combustion and Flame and Explosion Phenomena, Williams & Wilkins Co., 1949, pp. 266-288.

12. Hottel, H. C.; and Williams, G. C.: Measurements of Gas Composition (section C,6, pp. 62-73) and Measurement of Time-Dependent Properties (section C,8, pp. 82-88). Design and Performance of Gas Turbine Power Plants, W. R. Hawthorne and W. T. Olson, eds., Princeton Univ. Press, 1960.

13. Eggers, James M.; and Torrence, Marvin G.: An Experimental Investigation of the Mixing of Compressible-Air Jets in a Coaxial Configuration. NASA TN D-5315, 1969.

14. Anon.: U.S. Standard Atmosphere, 1962. NASA, U.S. Air Force, and U.S. Weather Bur., Dec. 1962.

15. Drell, Isadore L.; and Belles, Frank E.: Survey of Hydrogen Combustion Properties. NACA Rep. 1383, 1958. (Supersedes NACA RM E57D24.)

TABLE I.- RATIO OF PITOT PRESSURE TO NOZZLE PLENUM PRESSURE

MEASURED BY UNCOOLED RAKE

$\left[r_j = 1.09;\ p_{t,0} = 760\ kN/m^2\right]$

(a) Nonburning case

r/r_j	$p_{t,2}/p_{t,0}$ at x/r_j of –											
	0.00	2.33	4.65	6.98	9.30	11.63	13.95	16.28	18.60	20.92	23.24	25.00
2.48	0.6767	0.6709	0.6818	0.7040	0.7160	0.7055	0.7449	0.7297	0.7332	0.7042	0.6786	0.6657
2.66	.7047	.7121	.7048	.7339	.7450	.7363	.7742	.7655	.7537	.7333	.7154	.6950
2.87	.7172	.7313	.7173	.7454	.7566	.7517	.7732	.7859	.7557	.7430	.7319	.7106
3.15	.7172	.7313	.6847	.7522	.7546	.7556	.7654	.7888	.7449	.7430	.7454	.7135
3.37	.7056	.7054	.6568	.7416	.7334	.7402	.7381	.7646	.7263	.7285	.7387	.6998
3.60	.7269	.7256	.6923	.7647	.7469	.7633	.7527	.7733	.7478	.7449	.7541	.7203
3.88	.7360	.7263	.7225	.7344	.7520	.7703	.7630	.7716	.7556	.7499	.7496	.7257
4.11	.7379	.7263	.7365	.7363	.7567	.7722	.7687	.7640	.7565	.7508	.7496	.7276
4.32	.7398	.7254	.7356	.7372	.7604	.7703	.7763	.7480	.7556	.7527	.7487	.7352
4.58	.7379	.7282	.7403	.7091	.7651	.7665	.7839	.7395	.7565	.7537	.7487	.7418
4.81	.7407	.7263	.7337	.7156	.7717	.7562	.7792	.7386	.7556	.7555	.7487	.7504
5.05	.7426	.7254	.7337	.7241	.7727	.7543	.7696	.7395	.7527	.7527	.7468	.7485
5.28	.7388	.7347	.7346	.7297	.7482	.7600	.7639	.7414	.7556	.7537	.7449	.7466
5.54	.7307	.7368	.7263	.7322	.7412	.7594	.7481	.7352	.7489	.7448	.7334	.7327
5.75	.7279	.7321	.7282	.7379	.7307	.7670	.7385	.7362	.7498	.7438	.7343	.7308
6.03	.7250	.7321	.7301	.7417	.7174	.7727	.7326	.7314	.7373	.7352	.7276	.7211
6.21	.7279	.7321	.7320	.7341	.7183	.7679	.7113	.7112	.7006	.6949	.6894	.6912
6.43	.7241	.7340	.7330	.7313	7031	.6490	.6135	.6182	.5972	.6028	.6101	.6217
6.61	.7288	.7311	.7206	.6827	.5847	.4788	.4759	.4982	.4881	.5059	.5221	.5474

TABLE I.- RATIO OF PITOT PRESSURE TO NOZZLE PLENUM PRESSURE

MEASURED BY UNCOOLED RAKE – Concluded

(b) Burning case

r/r_j	$p_{t,2}/p_{t,0}$ at x/r_j of –															
	0.00	2.33	3.49	4.65	5.81	6.98	8.14	9.30	10.47	11.63	13.95	16.28	18.60	20.92	23.24	25.00
2.48	0.6777	0.6984	0.7157	0.7233	0.7154	0.7324	0.7391	0.7703	0.7595	0.7594	0.7605	0.7230	0.6797	0.5422	0.4020	0.2857
2.66	.7038	.7195	.7352	.7474	.7387	.7633	.7595	.7964	.7866	.7902	.8006	.7669	.7466	.7648	.6522	.4971
2.87	.7164	.7349	.7430	.7541	.7474	.7652	.7672	.7906	.7954	.7931	.8045	.7717	.7476	.7803	.7594	.5585
3.15	.7183	.7330	.7323	.7435	.7435	.7585	.7692	.7751	.7963	.7921	.7947	.7649	.7466	.7774	.7788	.7564
3.37	.7057	.7042	.7099	.7194	.7406	.7440	.7488	.7529	.7711	.7777	.7752	.7464	.7272	.7512	.7633	.7866
3.60	.7270	.7253	.7332	.7281	.7522	.7633	.7585	.7626	.7711	.7921	.7811	.7552	.7379	.7503	.7662	.7895
3.88	.7355	.7258	.7300	.7288	.7513	.7659	.7603	.7672	.7714	.8012	.7822	.7551	.7428	.7327	.7661	.7821
4.11	.7384	.7258	.7215	.7410	.7456	.7640	.7612	.7691	.7704	.7993	.7784	.7560	.7428	.7384	.7623	.7726
4.32	.7355	.7258	.7177	.7391	.7447	.7649	.7631	.7654	.7723	.7872	.7727	.7570	.7418	.7308	.7548	.7641
4.58	.7374	.7277	.7234	.7381	.7381	.7640	.7603	.7654	.7770	.7750	.7689	.7579	.7456	.7261	.7445	.7641
4.81	.7393	.7277	.7347	.7297	.7438	.7583	.7640	.7672	.7733	.7675	.7641	.7579	.7513	.7261	.7360	.7603
5.05	.7412	.7267	.7309	.7306	.7466	.7499	.7631	.7701	.7685	.7609	.7584	.7560	.7513	.7261	.7294	.7575
5.28	.7393	.7342	.7357	.7288	.7400	.7461	.7612	.7729	.7695	.7656	.7632	.7532	.7532	.7308	.7285	.7575
5.54	.7286	.7363	.7301	.7265	.7268	.7374	.7467	.7651	.7616	.7577	.7564	.7395	.7393	.7242	.7190	.7481
5.75	.7276	.7325	.7339	.7284	.7259	.7422	.7448	.7661	.7568	.7501	.7467	.7404	.7364	.7300	.7200	.7414
6.03	.7248	.7325	.7349	.7303	.7249	.7441	.7400	.7623	.7520	.7396	.7380	.7414	.7335	.7309	.7190	.7298
6.21	.7257	.7325	.7378	.7313	.7259	.7374	.7438	.7498	.7539	.7339	.7341	.7414	.7267	.7242	.7095	.7202
6.43	.7238	.7344	.7388	.7313	.7278	.7327	.7419	.7241	.7328	.7007	.6887	.7057	.6998	.6926	.6779	.6729
6.61	.7257	.7287	.7310	.7217	.7144	.6744	.6575	.6095	.6174	.6009	.5988	.6208	.6286	.6352	.6206	.6188

TABLE II.- PITOT PRESSURE AND CALCULATED MACH NUMBER AND FLOW DIRECTION AT $r/r_j = 3.37$

(a) Nonburning case

x/r_j	$p_{t,2}/p_{t,0}$	$p_{t,2}/p_{t,0}$ corrected	M	$\Delta\Theta$
0.00	0.7056	0.7055	2.033	0.000
2.33	.7054	.7055	2.033	.000
3.49		.7055	2.033	.000
4.07		.6812	2.085	-1.372
4.65	.6568	.6568	2.138	-2.657
5.23		.6568	2.138	-2.657
5.81		.6568	2.138	-2.657
6.40		.6568	1.998	.982
6.98	.7416	.7216	1.998	.982
7.56		.7196	2.003	.837
8.14		.7176	2.007	.722
8.72		.7155	2.011	.606
9.30	.7334	.7134	2.016	.477
9.88		.7151	2.012	.578
10.47		.7168	2.009	.664
11.05		.7185	2.005	.780
11.63	.7402	.7202	2.001	.895
12.21		.7196	2.003	.837
12.79		.7191	2.004	.809
13.37		.7186	2.005	.780
13.95	.7381	.7181	2.006	.751

(b) Burning case

x/r_j	$p_{t,2}/p_{t,0}$	$p_{t,2}/p_{t,0}$ corrected	M	$\Delta\Theta$
0.00	0.7057	0.7050	2.034	0.000
2.33	.7042	.7050	2.034	.000
2.91		.7075	2.029	.145
3.49	.7099	.7099	2.023	.304
4.07		.7147	2.013	.578
4.65	.7194	.7194	2.003	.867
5.23		.7200	2.002	.896
5.81	.7406	.7206	2.001	.925
6.40		.7223	1.997	1.041
6.98	.7440	.7240	1.993	1.157
7.56		.7264	1.988	1.301
8.14	.7488	.7288	1.983	1.446
8.72		.7309	1.978	1.605
9.30	.7529	.7329	1.974	1.720
9.88		.7320	1.976	1.663
10.47	.7711	.7311	1.978	1.605
11.05		.7344	1.971	1.807
11.63	.7777	.7377	1.964	2.024
12.21		.7371	1.965	1.995
12.79		.7365	1.966	1.952
13.37		.7359	1.968	1.894
13.95	.7752	.7352	1.969	1.865

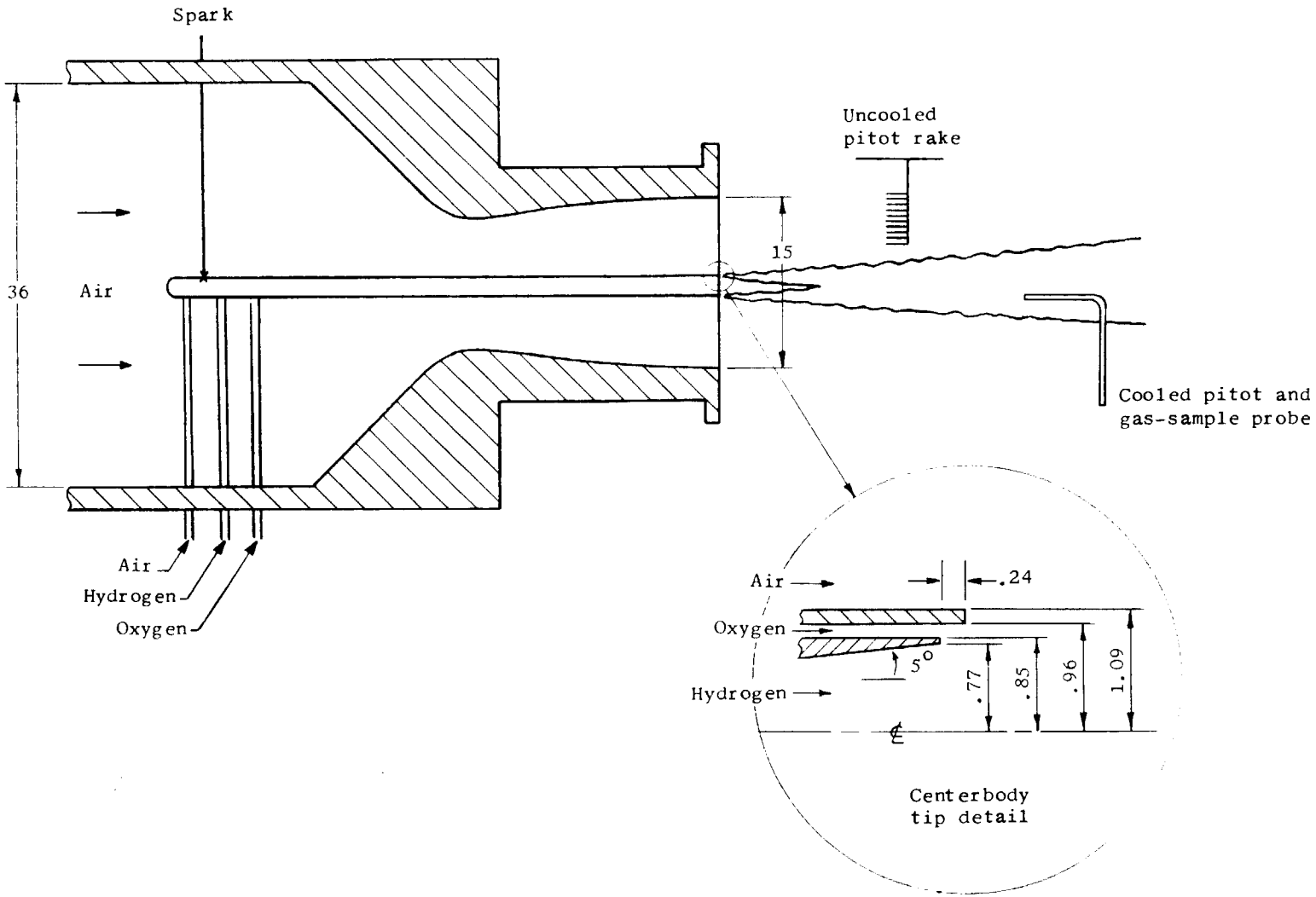

Figure 1.- Experimental apparatus. Dimensions are in centimeters.

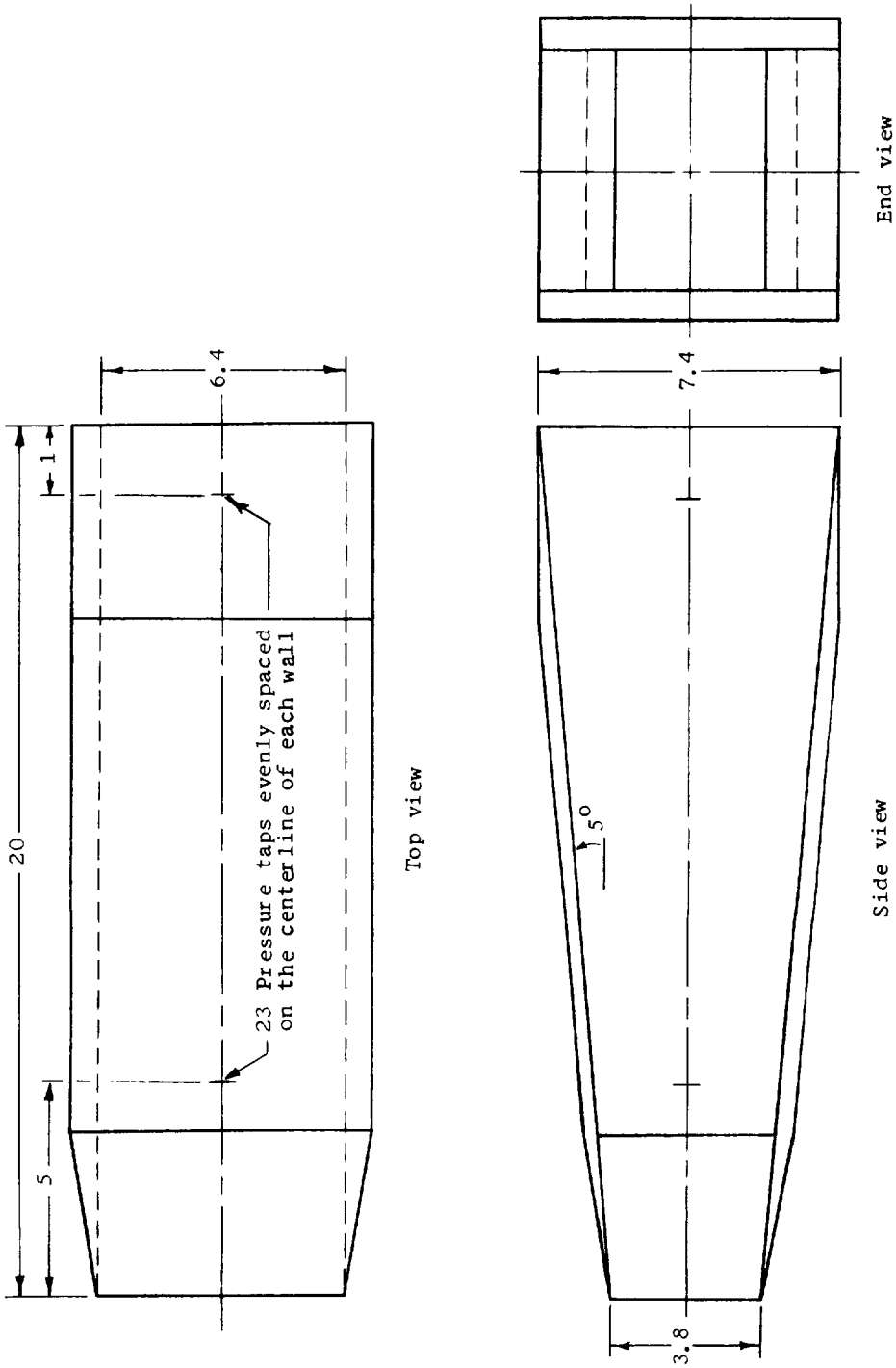

Figure 2.- Wave duct. Dimensions are in centimeters.

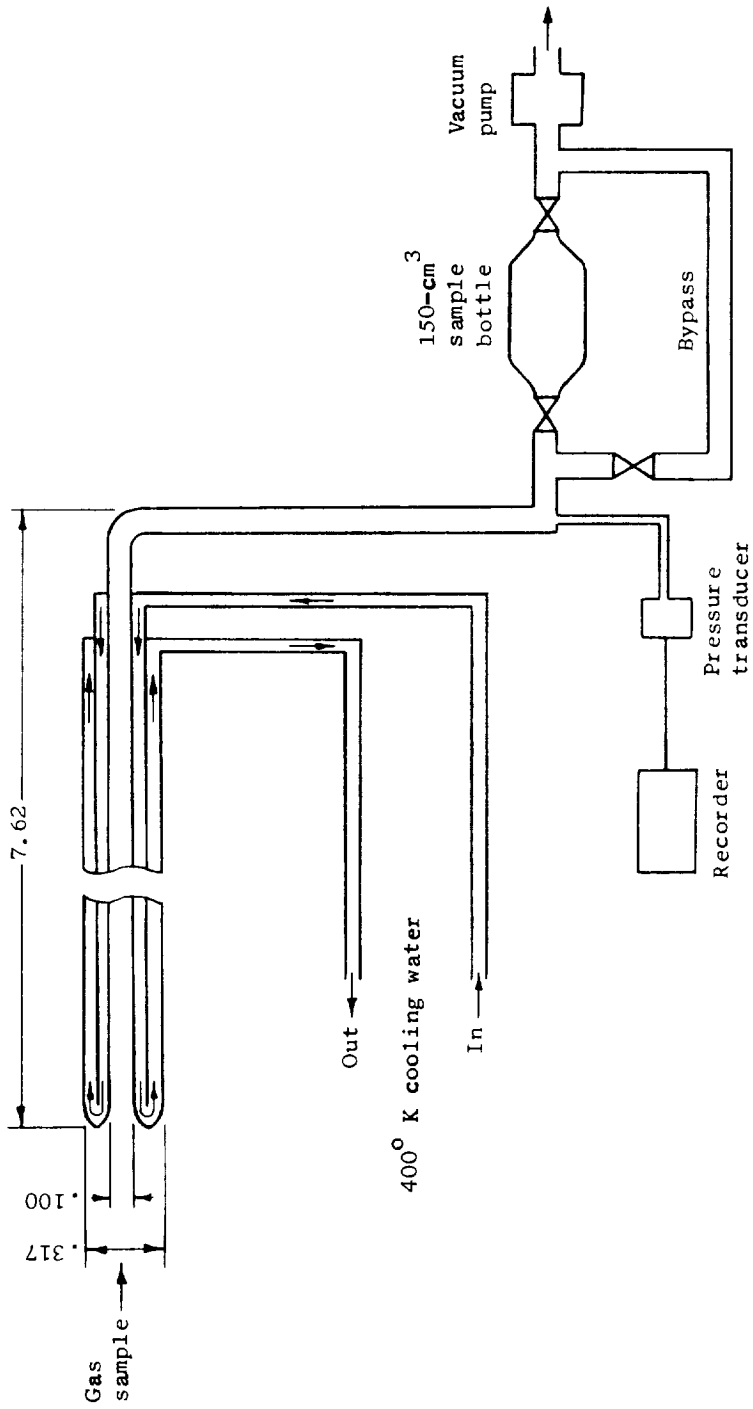

Figure 3.- Cooled probe and gas-sample collection system. Dimensions are in centimeters.

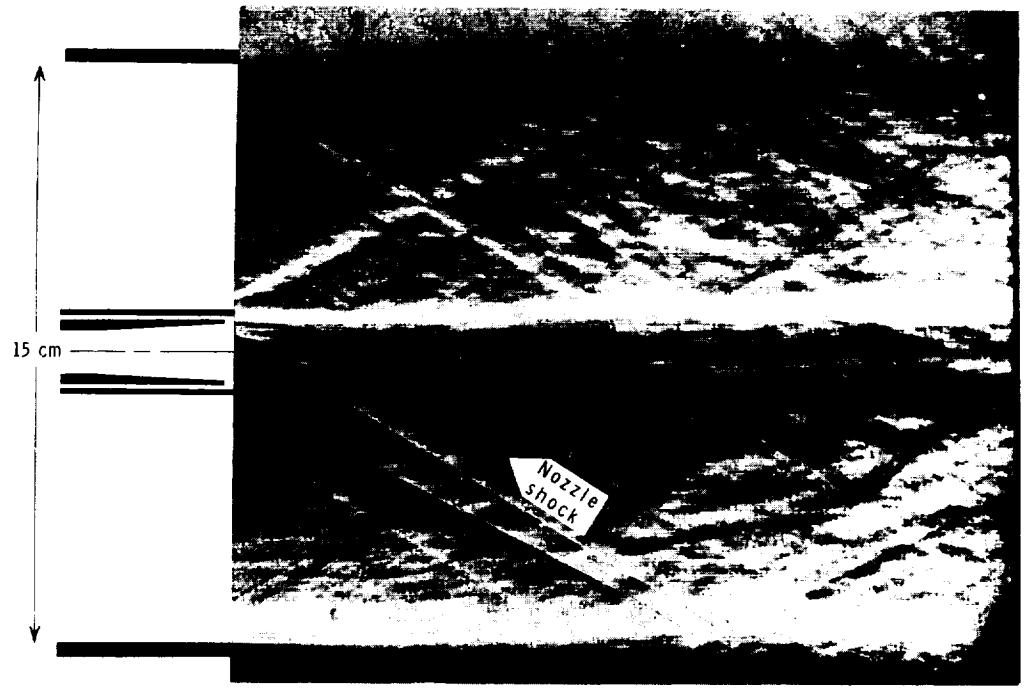

Nonburning

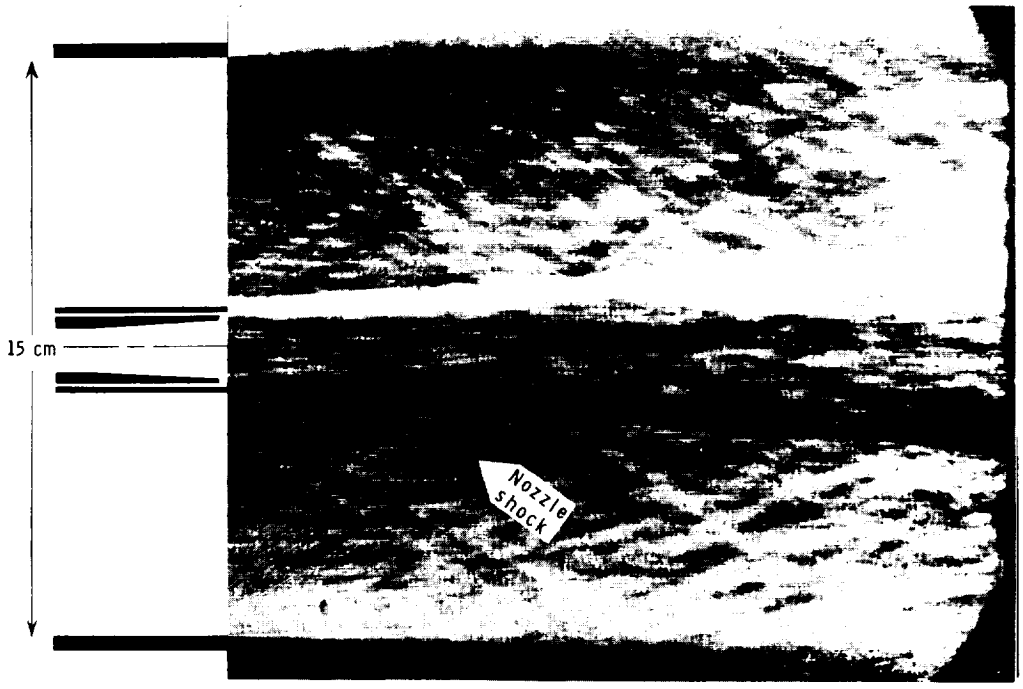

Burning

Figure 4.- Schlieren photographs of flow field.

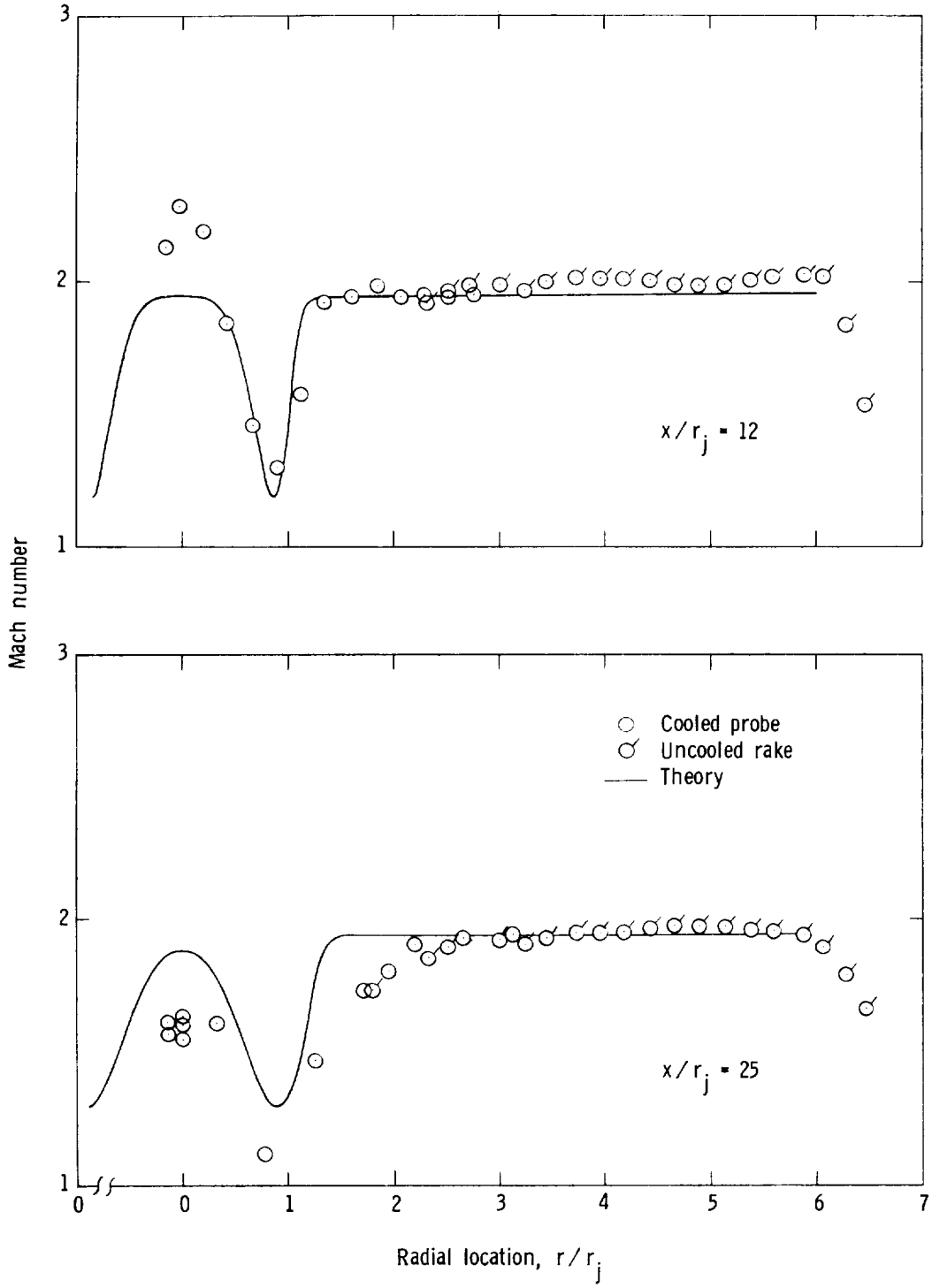

Figure 17.- Radial Mach number distribution for nonburning case.

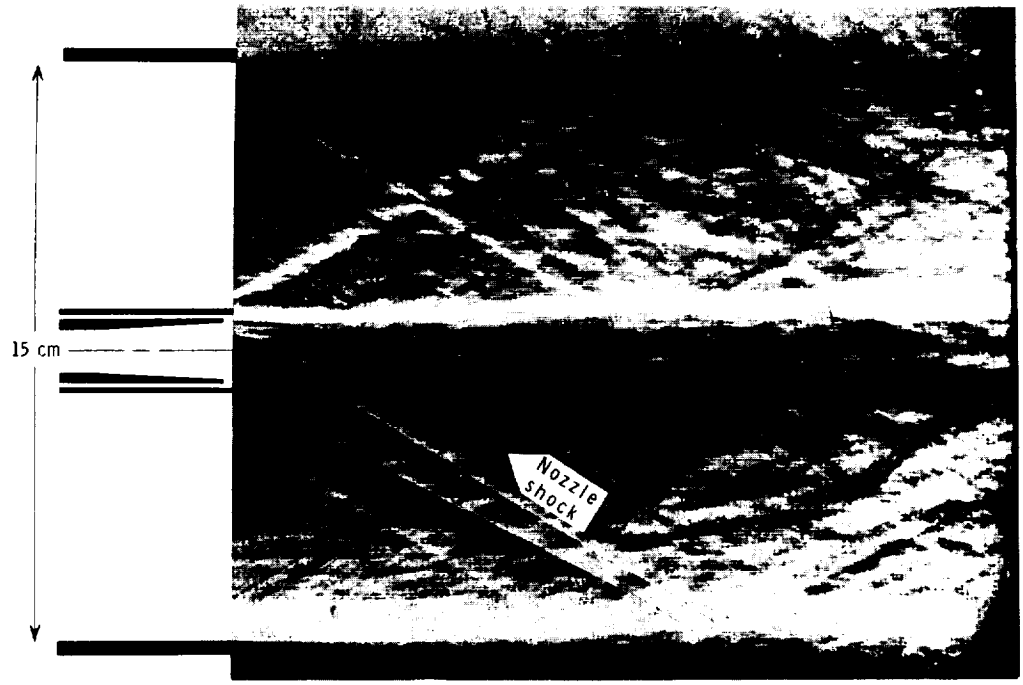

Nonburning

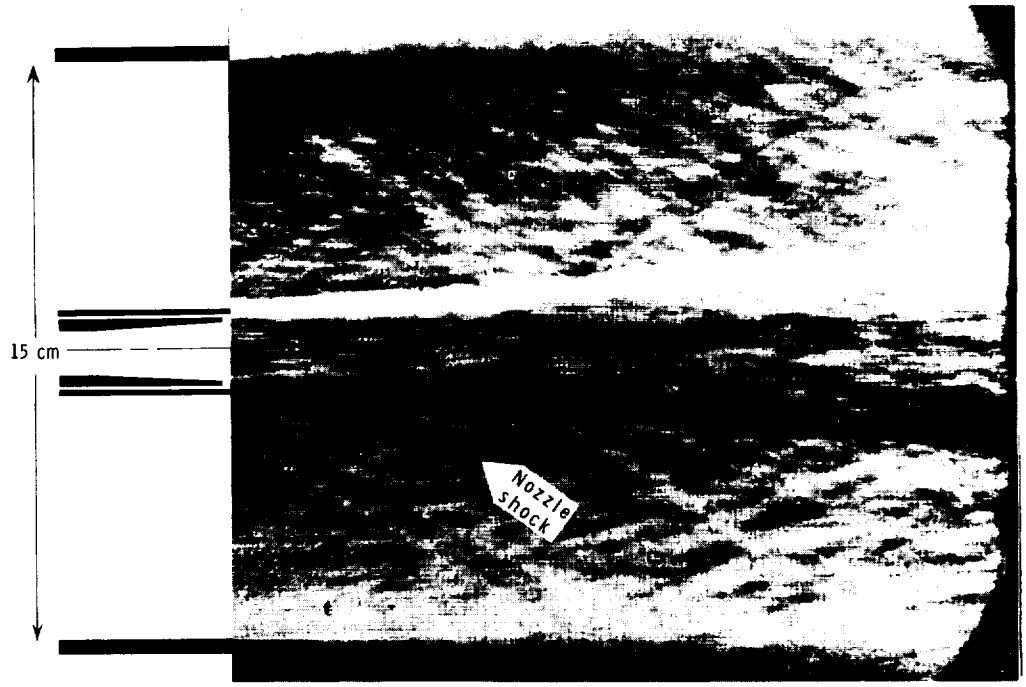

Burning

Figure 4.- Schlieren photographs of flow field.

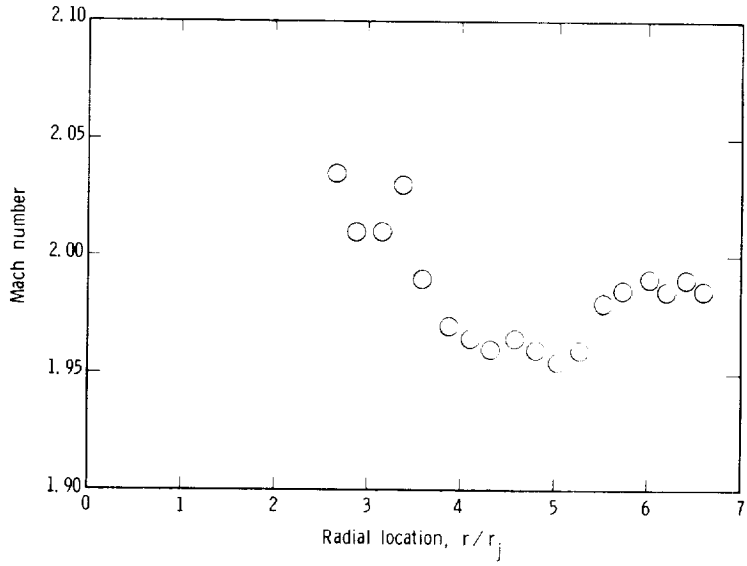

Figure 5.- Nozzle-exit Mach number profile.

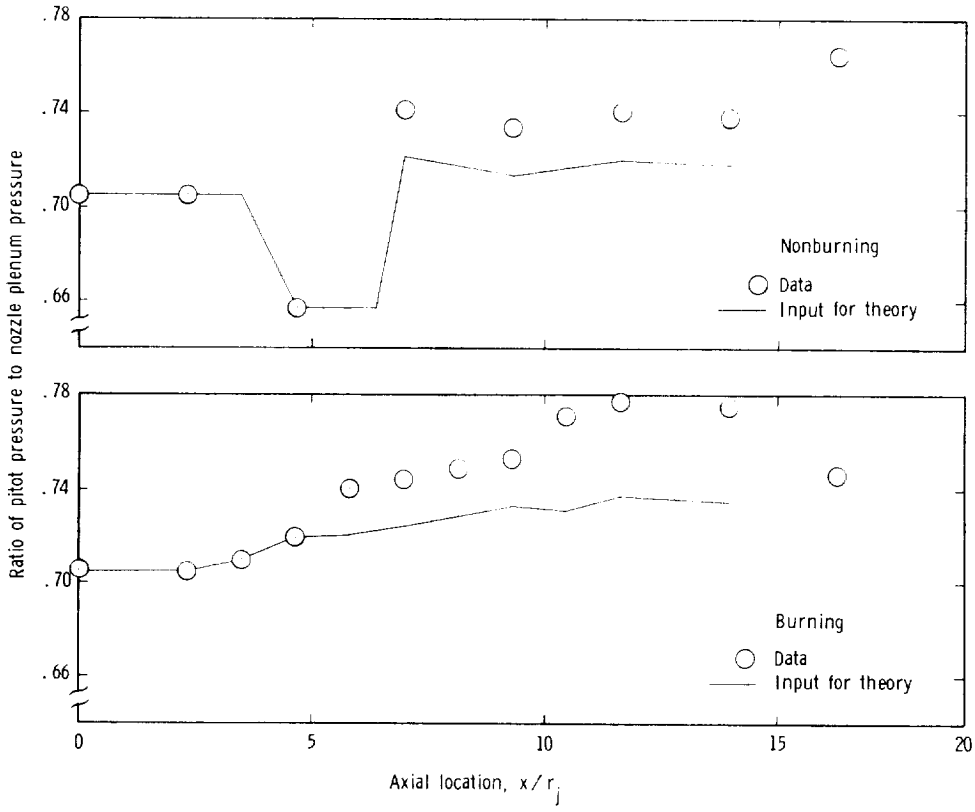

Figure 6.- Axial pitot-pressure distribution. $r/r_j = 3.37$.

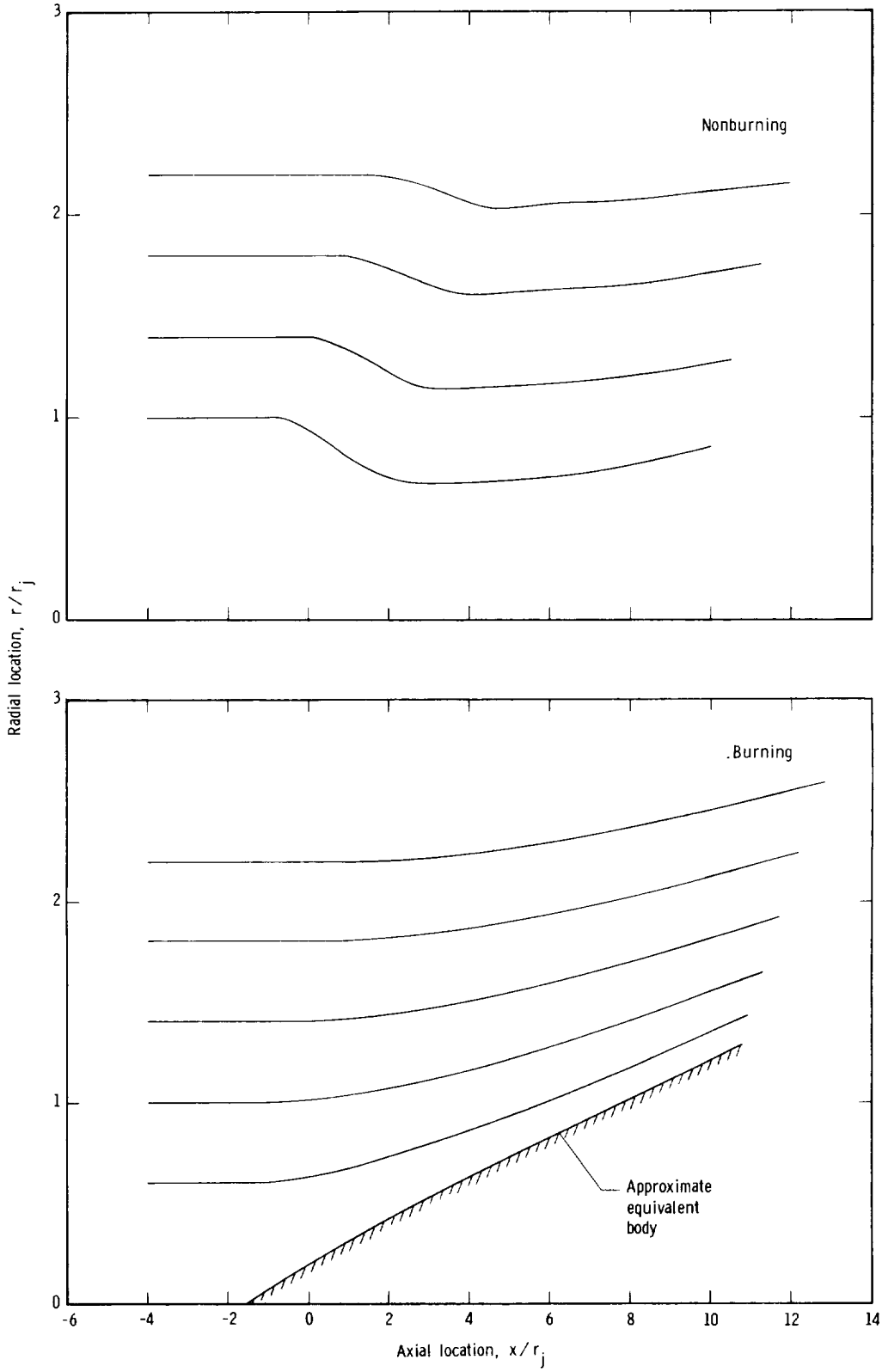

Figure 7.- Streamlines calculated by inverse application of method of characteristics.

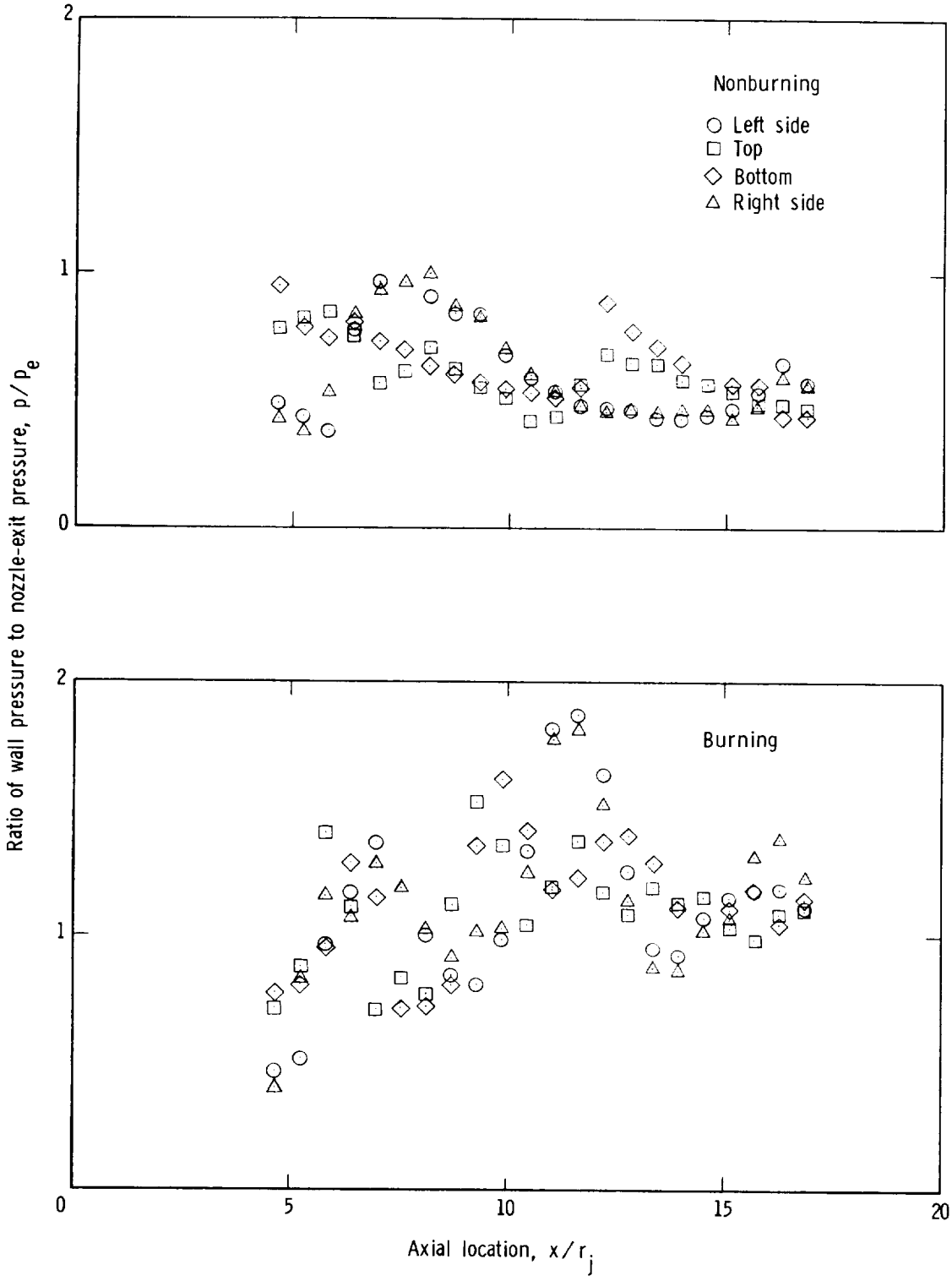

Figure 8.- Wave-duct static-pressure data.

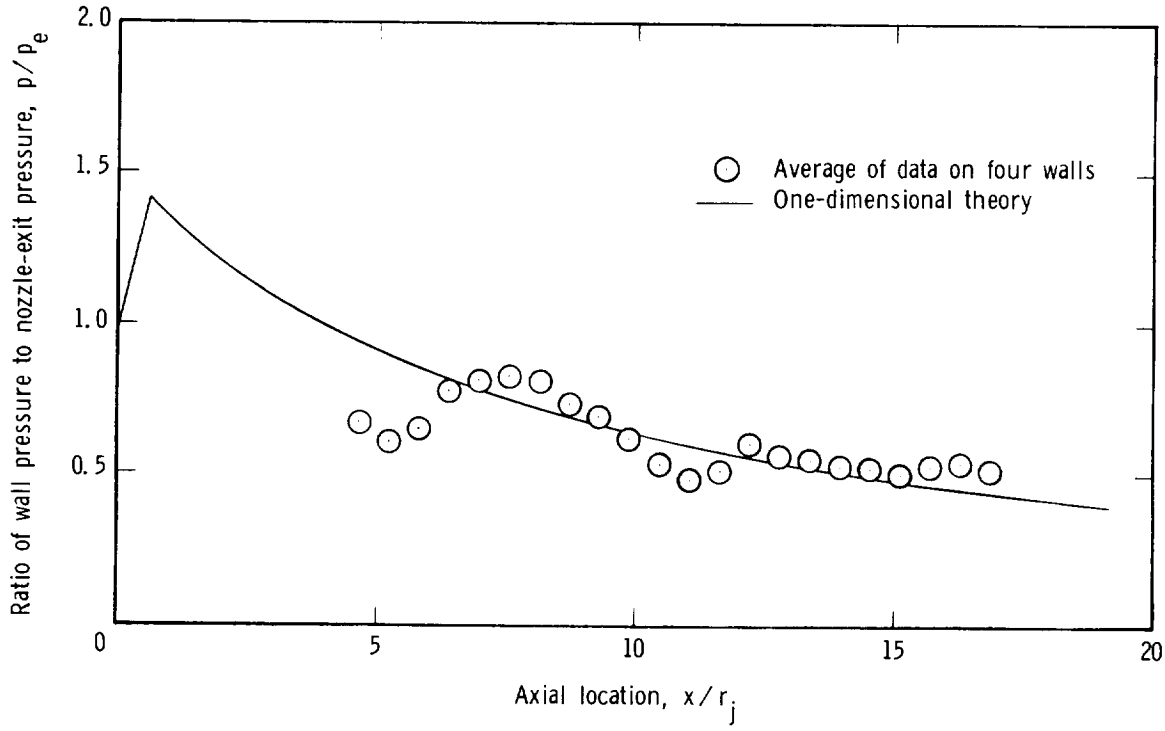

Figure 9.- Wave-duct average static-pressure data for nonburning case compared with one-dimensional theory.

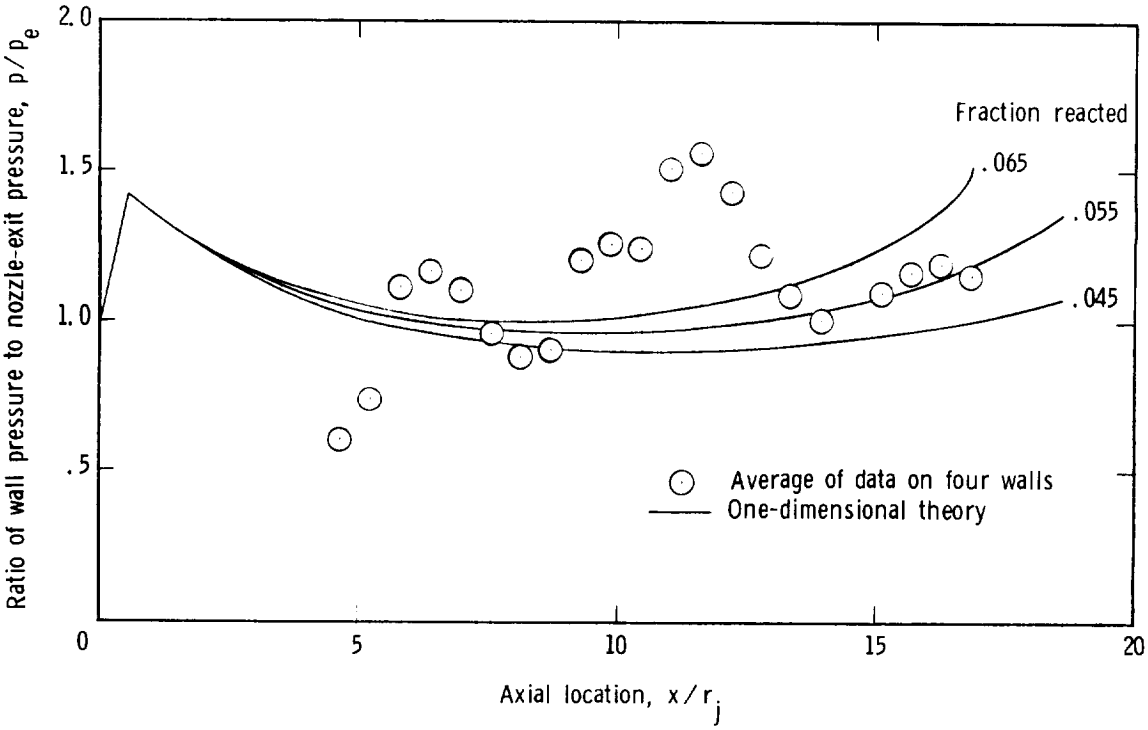

Figure 10.- Wave-duct average static-pressure data for burning case compared with one-dimensional theory.

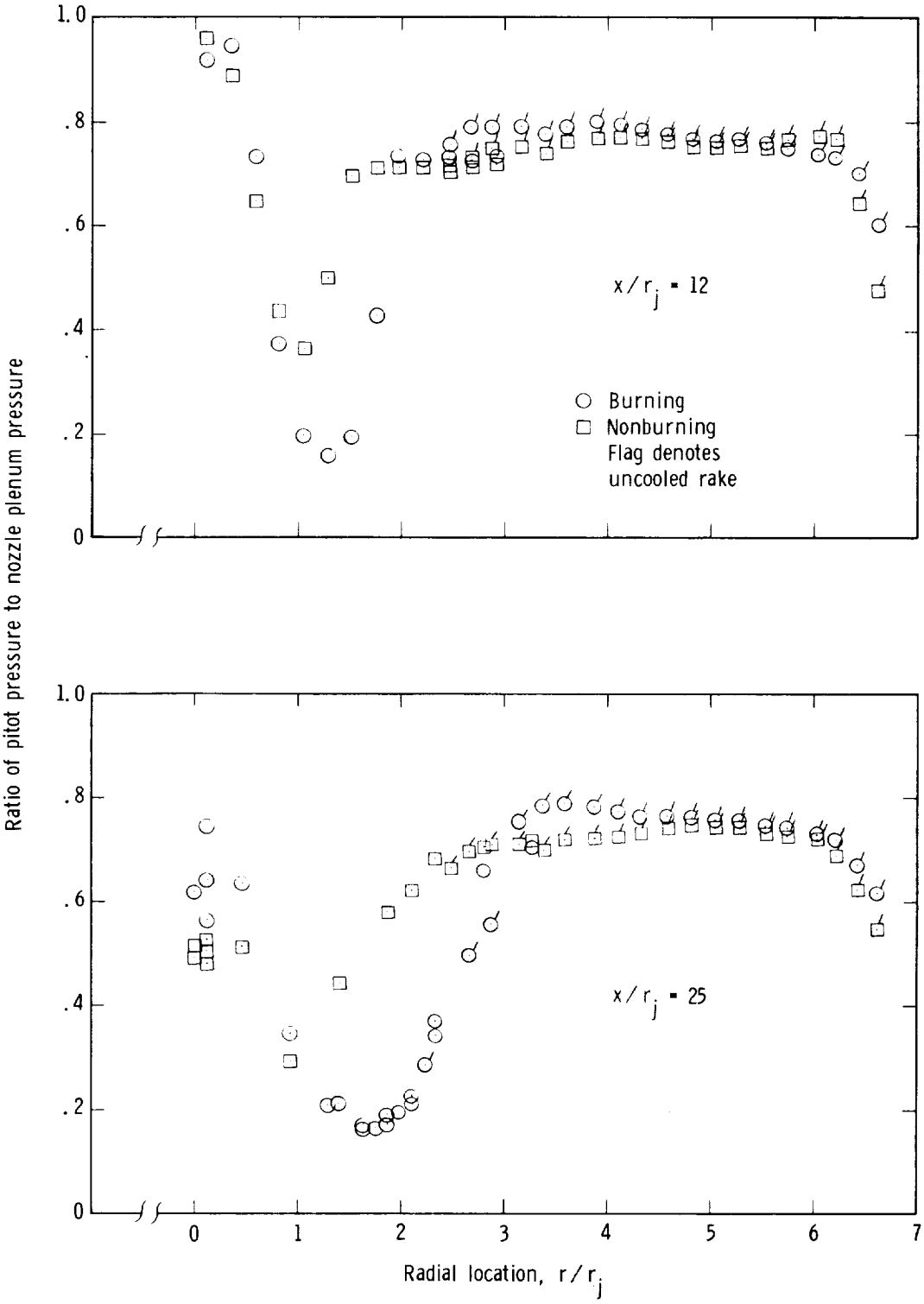

Figure 11.- Radial pitot-pressure distributions.

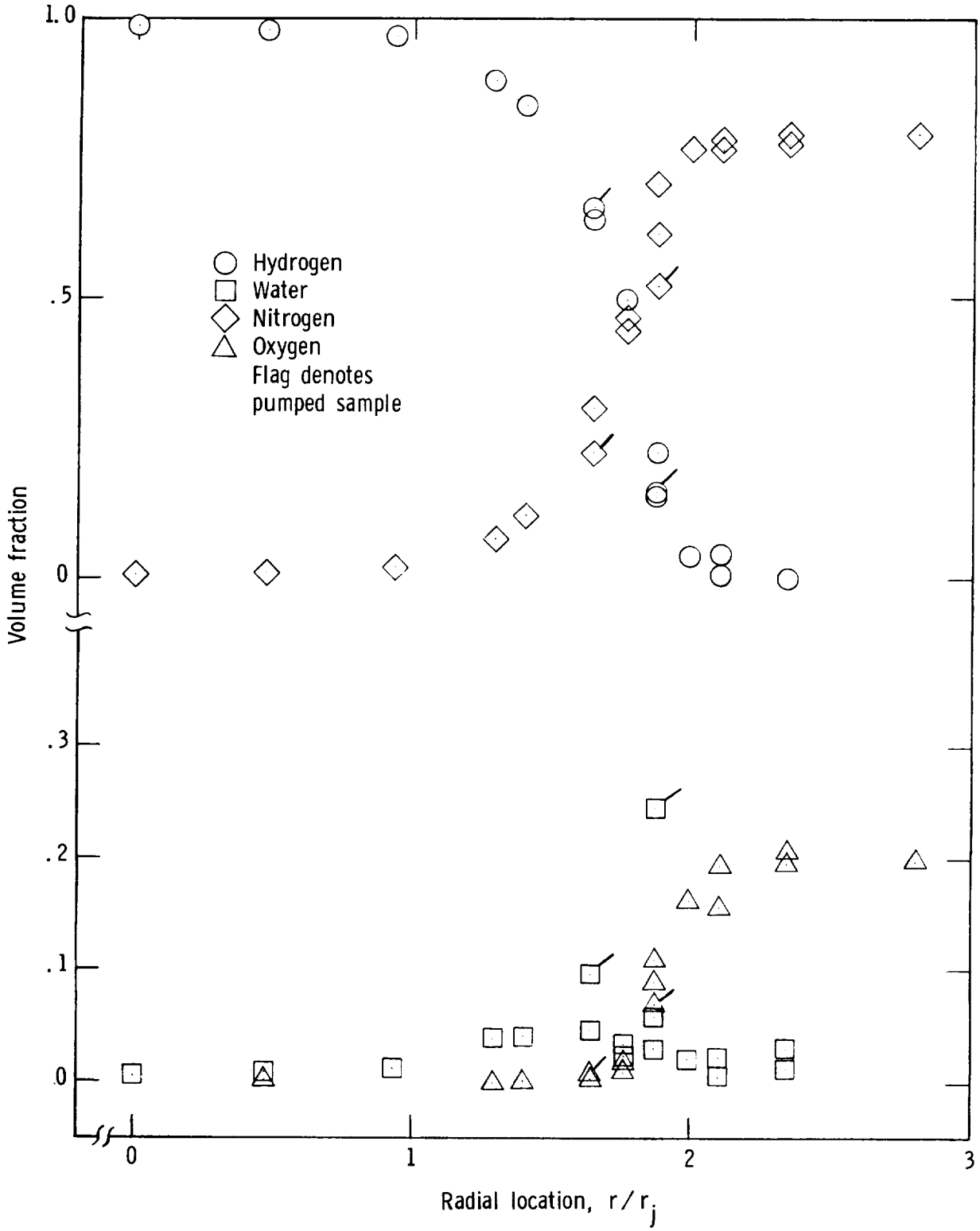

Figure 12.- Analysis of contents of gas-sample bottle. $x/r_j = 25$.

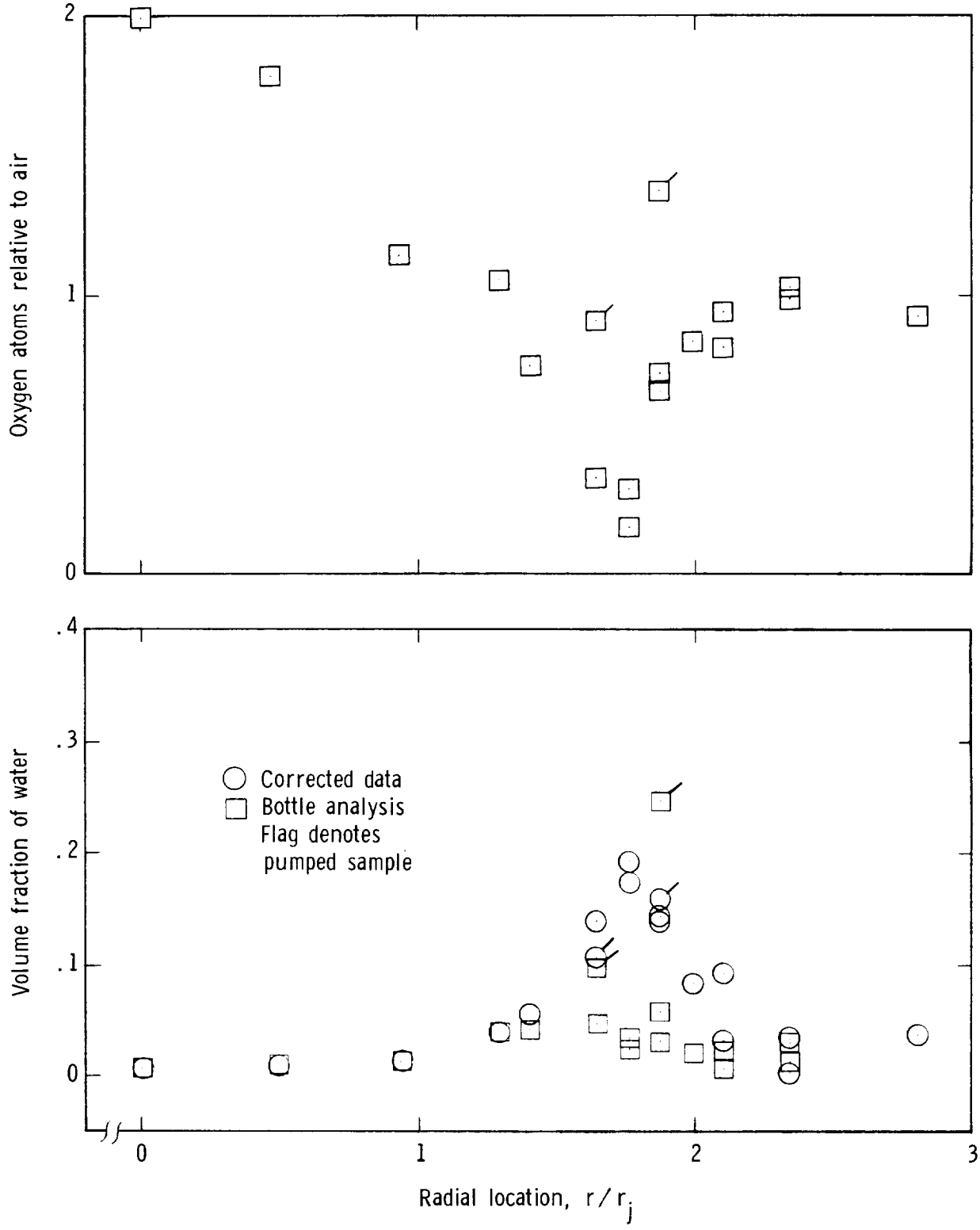

Figure 13.- Oxygen depletion and corrected water data. $x/r_j = 25$.

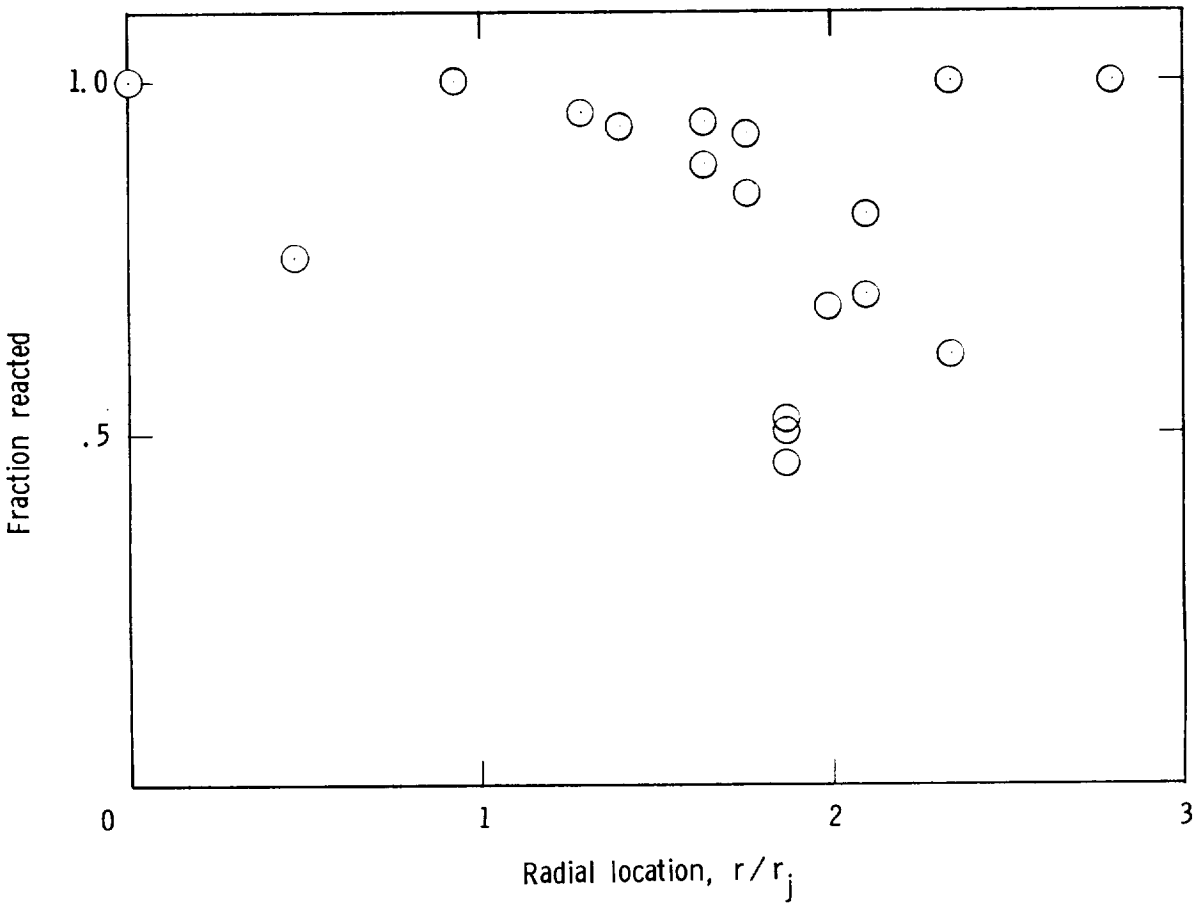

Figure 14.- Radial distribution of fraction reacted. $x/r_j = 25$.

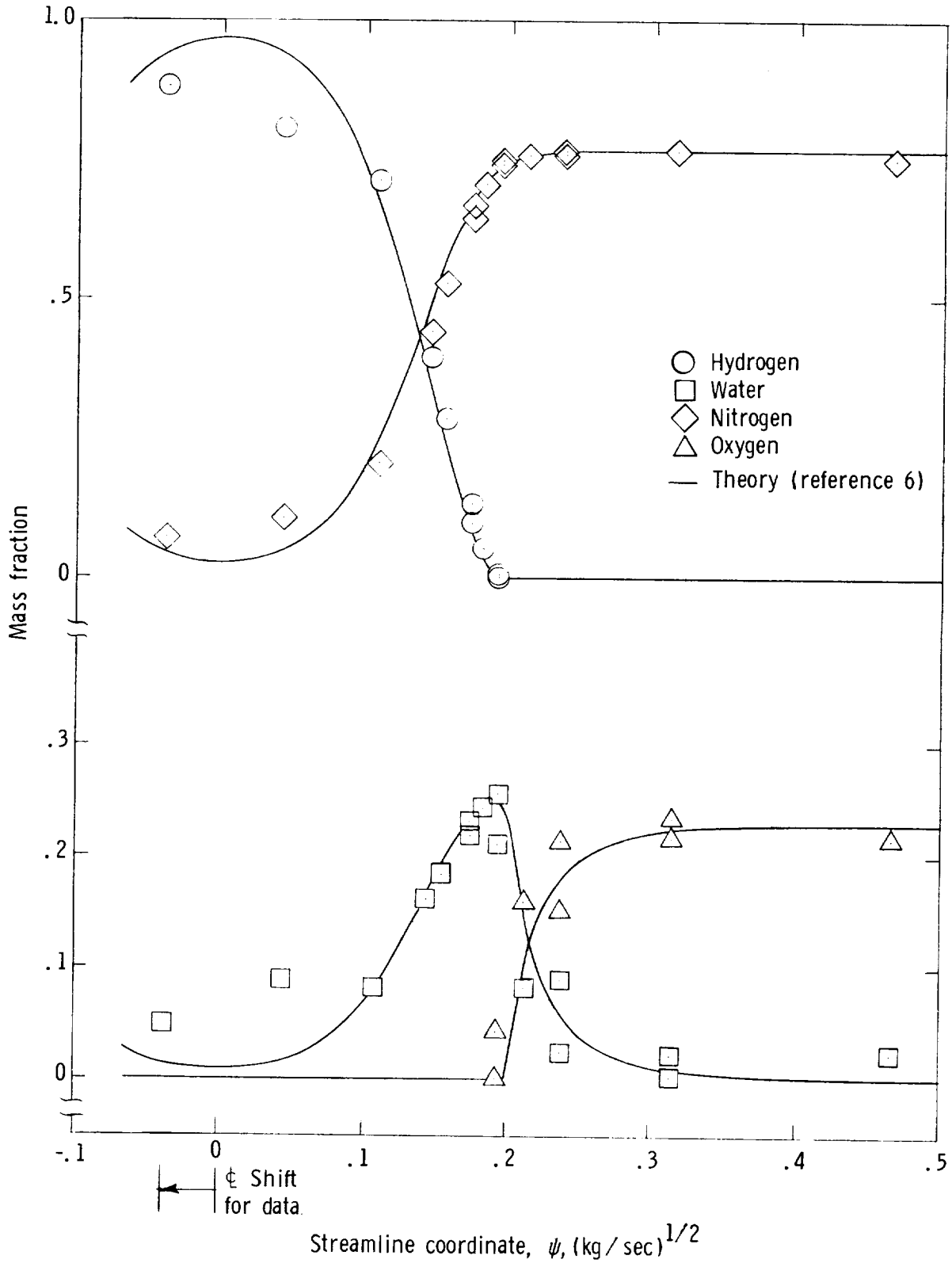

Figure 15.- Composition profiles compared with theory. $x/r_j = 25$.

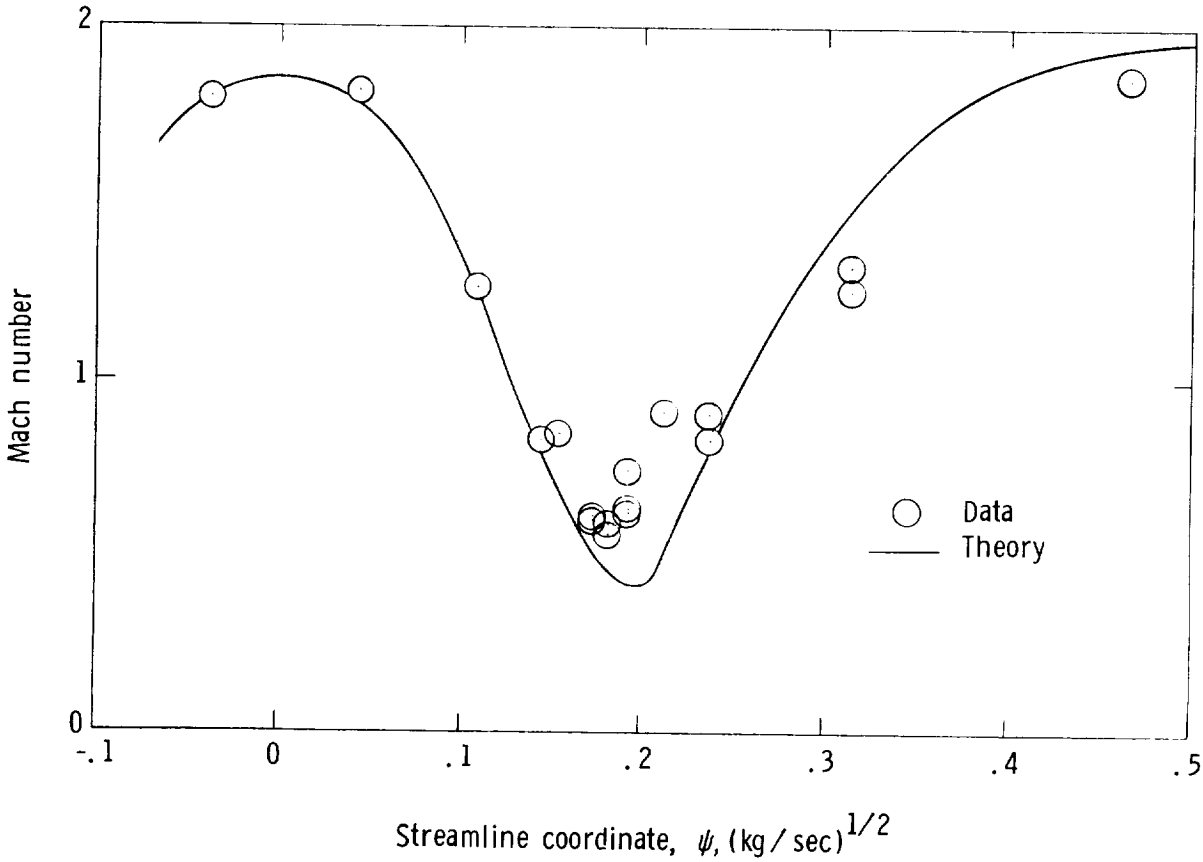

Figure 16.- Radial Mach number distribution for burning case. $x/r_j = 25$.

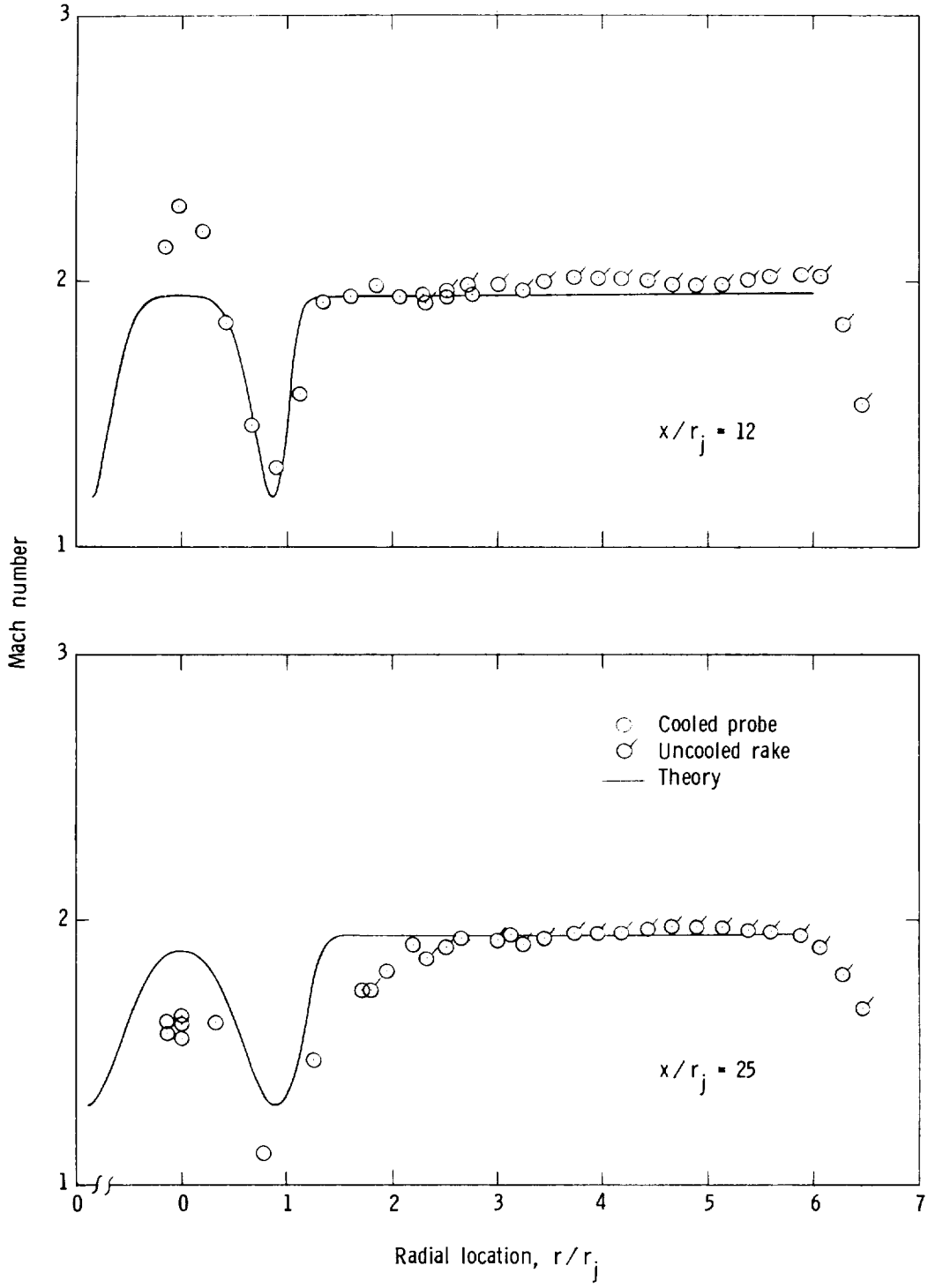

Figure 17.- Radial Mach number distribution for nonburning case.

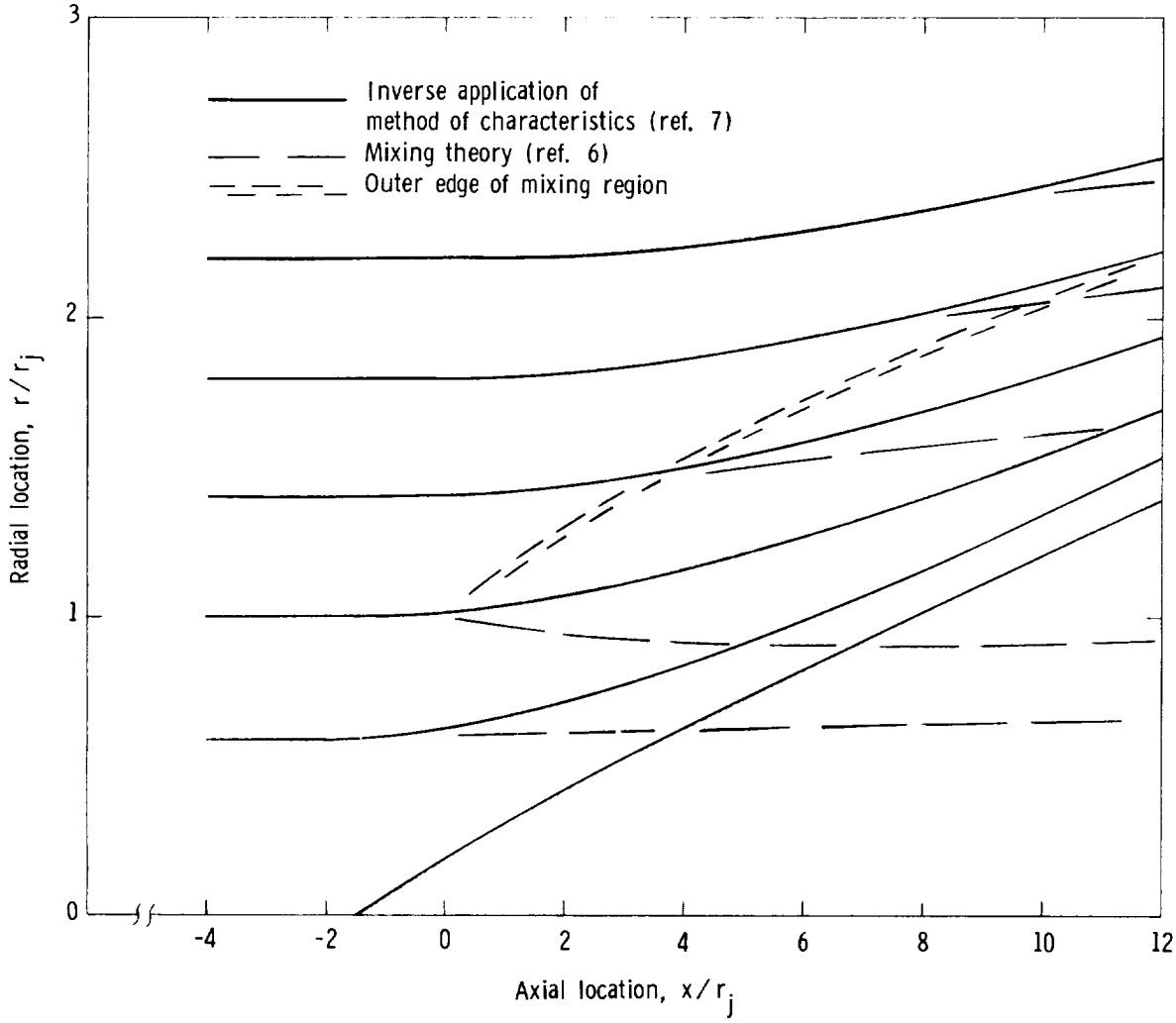

Figure 18.- Comparison of streamlines from mixing analysis and inverse application of method of characteristics for the burning case.